FOOL SHAP WITH STEALTHILY BIASED SAMPLING.

Gabriel Laberge[1], **Ulrich Aïvodji**[2], **Satoshi Hara**[3], **Mario Marchand**[4], **Foutse Khomh**[1]
[1]Polytechnique Montréal, Québec [2]École de technologie supérieure, Québec
[3]Osaka University, Japan [4]Universitié de Laval à Québec
{gabriel.laberge,foutse.khomh}@polymtl.ca
ulrich.aivodji@etsmtl.ca
satohara@ar.sanken.osaka-u.ac.jp
mario.marchand@ift.ulaval.ca

ABSTRACT

SHAP explanations aim at identifying which features contribute the most to the difference in model prediction at a specific input versus a background distribution. Recent studies have shown that they can be manipulated by malicious adversaries to produce arbitrary desired explanations. However, existing attacks focus solely on altering the black-box model itself. In this paper, we propose a complementary family of attacks that leave the model intact and manipulate SHAP explanations using stealthily biased sampling of the data points used to approximate expectations w.r.t the background distribution. In the context of fairness audit, we show that our attack can reduce the importance of a sensitive feature when explaining the difference in outcomes between groups while remaining undetected. These results highlight the manipulability of SHAP explanations and encourage auditors to treat them with skepticism.

1 INTRODUCTION

As Machine Learning (ML) gets more and more ubiquitous in high-stake decision contexts (e.g., healthcare, finance, and justice), concerns about its potential to lead to discriminatory models are becoming prominent. The use of auditing toolkits (Adebayo et al., 2016; Saleiro et al., 2018; Bellamy et al., 2018) is getting popular to circumvent the use of unfair models. However, although auditing toolkits can help model designers in promoting fairness, they can also be manipulated to mislead both the end-users and external auditors. For instance, a recent study of Fukuchi et al. (2020) has shown that malicious model designers can produce a benchmark dataset as fake "evidence" of the fairness of the model even though the model itself is unfair.

Another approach to assess the fairness of ML systems is to explain their outcome in a *post hoc* manner (Guidotti et al., 2018). For instance, `SHAP` (Lundberg & Lee, 2017) has risen in popularity as a means to extract model-agnostic local feature attributions. Feature attributions are meant to convey how much the model relies on certain features to make a decision at some specific input. The use of feature attributions for fairness auditing is desirable for cases where the interest is on the direct impact of the sensitive attributes on the output of the model. One such situation is in the context of causal fairness (Chikahara et al., 2021). In some practical cases, the outputs cannot be independent from the sensitive attribute unless we sacrifice much of prediction accuracy. For example, any decisions based on physical strength are statistically correlated to gender due to biological nature. The problem in such a situation is not the statistical bias (such as demographic parity), but whether the decision is based on the physical strength or gender, *i.e.* the attributions of each feature.

The focus of this study is on manipulating the feature attributions so that the dependence on sensitive attributions is hidden and the audits are misled as if the model is fair even if it is not the case. Recently, several studies reported that such a manipulation is possible, *e.g.* by modifying the black-box model to be explained (Slack et al., 2020; Begley et al., 2020; Dimanov et al., 2020), by manipulating the computation algorithms of feature attributions (Aïvodji et al., 2019), and by poisoning the data distribution (Baniecki et al., 2021; Baniecki & Biecek, 2022). With these findings in mind, the current possible advice to the auditors is not to rely solely on the reported feature attributions for fairness

auditing. A question then arises about what "evidence" we can expect in addition to the feature attributions, and whether they can be valid "evidence" of fairness.

In this study, we show that we can craft fake "evidence" of fairness for SHAP explanations, which provides the first negative answer to the last question. In particular, we show that we can produce not only manipulated feature attributions but also a benchmark dataset as the fake "evidence" of fairness. The benchmark dataset ensures the external auditors reproduce the reported feature attributions using the existing SHAP library. In our study, we leverage the idea of stealthily biased sampling introduced by Fukuchi et al. (2020) to cherry-pick which data points to be included in the benchmark. Moreover, the use of stealthily biased sampling allows us to keep the manipulation undetected by making the distribution of the benchmark sufficiently close to the true data distribution. Figure 1 illustrates the impact of our attack in an explanation scenario with the Adult Income dataset.

Our contributions can be summarized as follows:

- Theoretically, we formalize a notion of foreground distribution that can be used to extend Local Shapley Values (LSV) to Global Shapley Values (GSV), which can be used to decompose fairness metrics among the features (Section 2.2). Moreover, we formalize the task of manipulating the GSV as a Minimum Cost Flow (MCF) problem (Section 4).
- Experimentally (Section 5), we illustrate the impact of the proposed manipulation attack on a synthetic dataset and four popular datasets, namely Adult Income, COMPAS, Marketing, and Communities. We observed that the proposed attack can reduce the importance of a sensitive feature while keeping the data manipulation undetected by the audit.

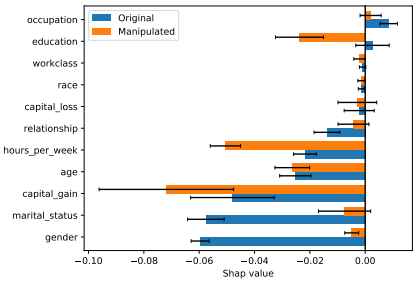

Figure 1: Example of our attack on the Adult Income dataset. After the attack, the feature gender moved from the most negative attribution to the 6^{th}, hence hiding some of the explicit model bias.

Our results indicate that SHAP explanations are not robust and can be manipulated when it comes to explaining the difference in outcomes between groups. Even worse, our results confirm we can craft a benchmark dataset so that the manipulated feature attributions are reproducible by external audits. Henceforth, we alert auditors to treat post-hoc explanations methods with skepticism even if it is accompanied by some additional evidence.

2 Shapley Values

2.1 Local Shapley Values

Shapley values are omnipresent in post-hoc explainability because of their fundamental mathematical properties (Shapley, 1953) and their implementation in the popular SHAP Python library (Lundberg & Lee, 2017). SHAP provides local explanations in the form of feature attributions i.e. given an input of interest $\boldsymbol{x}$, SHAP returns a score $\phi_i \in \mathbb{R}$ for each feature $i = 1, 2, \ldots, d$. These scores are meant to convey how much the model f relies on feature i to make its decision $f(\boldsymbol{x})$. Shapley values have a long background in coalitional game theory, where multiple players collaborate toward a common outcome. In the context of explaining model decisions, the players are the input features and the common outcome is the model output $f(\boldsymbol{x})$ which we are trying to explain. In coalitional games, players (features) are either present or absent. Since one cannot physically remove an input feature once the model has already been fitted, SHAP removes features by replacing them with a baseline value $\boldsymbol{z}$. This leads to the *Local Shapley Value* (LSV) $\phi_i(f, \boldsymbol{x}, \boldsymbol{z})$ which respect the so-called efficiency axiom (Lundberg & Lee, 2017)

$$\sum_{i=1}^{d} \phi_i(f, \boldsymbol{x}, \boldsymbol{z}) = f(\boldsymbol{x}) - f(\boldsymbol{z}). \tag{1}$$

Simply put, the difference between the model prediction at $\boldsymbol{x}$ and the baseline $\boldsymbol{z}$ is shared among the different features. Additional details on the computation of LSV are presented in Appendix B.1.

2.2 GLOBAL SHAPLEY VALUES

LSV are local in the sense that they explain the prediction at a specific $\boldsymbol{x}$ and rely on a single baseline input $\boldsymbol{z}$. Since model auditing requires a more global analysis of model behavior, we must understand the predictions at multiple inputs $\boldsymbol{x} \sim \mathcal{F}$ sampled from a distribution $\mathcal{F}$ called the *foreground*. Moreover, because the choice of baseline is somewhat ambiguous, the baselines are sampled $\boldsymbol{z} \sim \mathcal{B}$ from a distribution $\mathcal{B}$ colloquially referred to as the *background*. Taking inspiration from Begley et al. (2020), we can compute *Global Shapley Values* (GSV) by averaging LSV over both foreground and background distributions.

Definition 2.1.

$$\Phi_i(f, \mathcal{F}, \mathcal{B}) := \mathop{\mathbb{E}}_{\substack{\boldsymbol{x}\sim\mathcal{F} \\ \boldsymbol{z}\sim\mathcal{B}}}\big[\phi_i(f, \boldsymbol{x}, \boldsymbol{z})\big], \quad i = 1, 2, \ldots, d. \tag{2}$$

Proposition 2.1. *The GSV have the following property*

$$\sum_{i=1}^{d} \Phi_i(f, \mathcal{F}, \mathcal{B}) = \mathop{\mathbb{E}}_{\boldsymbol{x}\sim\mathcal{F}}[f(\boldsymbol{x})] - \mathop{\mathbb{E}}_{\boldsymbol{x}\sim\mathcal{B}}[f(\boldsymbol{x})]. \tag{3}$$

This is a direct result of Equation 1.

2.3 MONTE-CARLO ESTIMATES

In practice, computing the expectations w.r.t the whole background and foreground distributions may be prohibitive and hence Monte-Carlo estimates are used. For instance, when a dataset is used to represent a background distribution, many explainers in the `SHAP` library such as the `ExactExplainer` and `TreeExplainer` will subsample this dataset[1] by selecting 100 instances uniformly at random when the size of the dataset exceeds 100. More formally, let

$$\mathcal{C}(S, \boldsymbol{\omega}) := \sum_{\boldsymbol{x}^{(j)}\in S} \omega_j \delta(\boldsymbol{x}^{(j)}) \tag{4}$$

represent a categorical distribution over a finite set of input examples S, where $\delta(\cdot)$ is the dirac probability measure, $w_j \geqslant 0 \ \forall j$, and $\sum_j \omega_j = 1$. Estimating expectations with Monte-Carlo amounts to sampling M instances

$$S_0 \sim \mathcal{F}^M \qquad S_1 \sim \mathcal{B}^M, \tag{5}$$

and compute the plug-in estimates

$$\begin{aligned} \widehat{\boldsymbol{\Phi}}(f, S_0, S_1) &:= \boldsymbol{\Phi}(f, \mathcal{C}(S_0, \mathbf{1}/M), \mathcal{C}(S_1, \mathbf{1}/M)) \\ &= \frac{1}{M^2} \sum_{\boldsymbol{x}^{(i)}\in S_0} \sum_{\boldsymbol{z}^{(j)}\in S_1} \boldsymbol{\phi}(f, \boldsymbol{x}^{(i)}, \boldsymbol{z}^{(j)}). \end{aligned} \tag{6}$$

When a set of samples is a singleton (*e.g.* $S_1 = \{\boldsymbol{z}^{(j)}\}$), we shall use the convention $\widehat{\boldsymbol{\Phi}}(f, S_0, \{\boldsymbol{z}^{(j)}\}) \equiv \widehat{\boldsymbol{\Phi}}(f, S_0, \boldsymbol{z}^{(j)})$ to improve readability. In Appendix B.2, $\widehat{\boldsymbol{\Phi}}(f, S_0, S_1)$ is shown to be a consistent and asymptotically normal estimate of $\boldsymbol{\Phi}(f, \mathcal{F}, \mathcal{B})$ meaning that one can compute approximate confidence intervals around $\widehat{\boldsymbol{\Phi}}$ to capture $\boldsymbol{\Phi}$ with high probability. In practice, the estimates $\widehat{\boldsymbol{\Phi}}$ are employed as the model explanation which we see as a vulnerability. As discussed in Section 4, the Monte-Carlo estimation is the key ingredient that allow us to manipulate the GSV in favor of a dishonest entity.

[1] https://github.com/slundberg/shap/blob/0662f4e9e6be38e658120079904899cccda59ff8/shap/maskers/_tabular.py#L54-L55

3 AUDIT SCENARIO

This section introduces an audit scenario to which the proposed attack of SHAP can apply. This scenario involves two parties: a company and an audit. The company has a dataset $D = \{(\boldsymbol{x}^{(i)}, y^{(i)})\}_{i=1}^{N}$ with $\boldsymbol{x}^{(i)} \in \mathbb{R}^d$ and $y^{(i)} \in \{0, 1\}$ that contains N input-target tuples and also has a model $f : \mathcal{X} \to [0, 1]$ that is meant to be deployed in society. The binary feature with index s (*i.e* $x_s \in \{0, 1\}$) represents a sensitive feature with respect to which the model should not explicitly discriminate. Both the data D and the model f are highly private so the company is very careful when providing information about them to the audit. Hence, f is a black box from the point of view of the audit. At first, the audit asks the company for the necessary data to compute fairness metrics *e.g.* the Demographic Parity (Dwork et al., 2012), the Predictive Equality (Corbett-Davies et al., 2017), or the Equal Opportunity (Hardt et al., 2016). Note that our attack would apply as long as the fairness metric is a difference in model expectations over subgroups. For simplicity, the audit decides to compute the Demographic Parity

$$\mathbb{E}[f(\boldsymbol{x})|x_s = 0] - \mathbb{E}[f(\boldsymbol{x})|x_s = 1], \tag{7}$$

and henceforth demands access to the model outputs for all inputs with different values of the sensitive feature *i.e* $f(D_0)$ and $f(D_1)$, where $D_0 = \{\boldsymbol{x}^{(i)} : x_s^{(i)} = 0\}$ and $D_1 = \{\boldsymbol{x}^{(i)} : x_s^{(i)} = 1\}$ are subsets of the input data of sizes N_0 and N_1 respectively. Doing so does not force the company to share values of features other than x_s nor does it requires direct access to the inner workings of the proprietary model. Hence this demand respects privacy requirements and the company will accept to share the model outputs across all instances, see Figure 2a. At this point, the audit confirms that the model is indeed biased in favor of $x_s = 1$ and puts in question the ability of the company to deploy such a model. Now, the company argues that, although the model exhibits a disparity in outcomes, it does not mean that the model explicitly uses the feature x_s to make its decision. If such is the case, then the disparity could be explained by other features statistically associated with x_s. Some of these other features may be acceptable grounds for decisions. To verify such a claim, the audit decides to employ post-hoc techniques to explain the disparity. Since the model is a black-box, the audits shall compute the GSVs. The foreground $\mathcal{F}$ and background $\mathcal{B}$ are chosen to be the data distributions conditioned on $x_s = 0$ and $x_s = 1$ respectively

$$\mathcal{F} := \mathcal{C}(D_0, \mathbf{1}/N_0) \qquad \mathcal{B} := \mathcal{C}(D_1, \mathbf{1}/N_1). \tag{8}$$

According to Equation 3, the resulting GSVs will sum up of the demographic parity (cf. Equation 7). If the sensitive feature has a large negative GSV Φ_s, then this would mean that the model is **explicitly** relying on x_s to make its decisions and the company would be forbidden from deploying the model. If the GSV has a small amplitude, however, the company could still argue in favour of deploying the model in spite of having disparate outcomes. Indeed, the difference in outcomes by the model could be attributed to other more acceptable features. See Figure 2b for a toy example illustrating this reasoning.

To compute the GSV, the audit demands the two datasets of inputs D_0 and D_1, as well as the ability to query the black box f at arbitrary points. Because of privacy concerns on sharing values of $\boldsymbol{x}$ across the whole dataset, and because GSV must be estimated with Monte-Carlo, both parties agree that the company shall only provide subsets $S_0 \subset D_0$ and $S_1 \subset D_1$ of size M to the audit so they can compute a Monte-Carlo estimate $\widehat{\boldsymbol{\Phi}}(f, S_0, S_1)$. The company first estimate GSV on their own by choosing S_0, S_1 uniformly at random from $\mathcal{F}$ and $\mathcal{B}$ (cf. Equation 5) and observe that $\widehat{\Phi}_s$ indeed has a large negative value. They realize they must carefully select which data points will be sent, otherwise, the audit may observe the explicit bias toward $x_s = 1$ and the model will not be deployed. Moreover, the company understands that the audit currently has access to the data $f(D_0)$ and $f(D_1)$ representing the model predictions on the whole dataset (see Figure 2a). Therefore, if the company does not share subsets S_0, S_1 that where chosen uniformly at random from D_0, D_1, it is possible for the audit to detect this fraud by doing a statistical test comparing $f(S_0)$ to $f(D_0)$ and $f(S_1)$ to $f(D_1)$. The company needs a method to select **misleading subsets** S_0', S_1' in a manner that manipulates the GSV in their favour, while remaining undetected by the audit. Such a method is the subject of the next section.

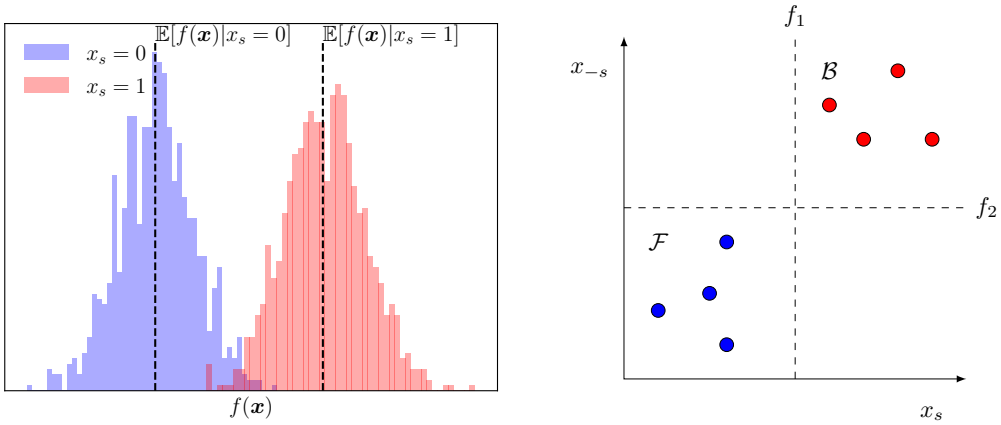

(a) The data initially provided by the company to the audit is $f(D_0)$ and $f(D_1)$ *i.e* the model predictions for all instances in the private dataset for different values of x_s. This dataset can later be used by the audit to assess whether or not the subsets S'_0, S'_1 provided by the company where cherry-picked.

(b) Two models f_1 and f_2 (decision boundaries in dashed lines) with perfect accuracy exhibit a disparity in outcomes w.r.t groups with $x_s < 0$ and $x_s > 0$. Here, $\Phi_s(f_1, \mathcal{F}, \mathcal{B}) = -1$ while $\Phi_s(f_2, \mathcal{F}, \mathcal{B}) = 0$. Hence, f_2 is **indirectly** unfair toward x_s because of correlations in the data.

Figure 2: Illustrations of the audit scenario.

4 Fool SHAP with Stealthily Biased Sampling

4.1 Manipulation

To fool the audit, the company can decide to indeed sample S'_0 uniformly at random $S'_0 \sim \mathcal{F}^M$. Then, given this choice of foreground sub-sample, they can manipulate the background distribution to cherry-pick M instances. Formally, the company must compute a non-uniform background distribution $\mathcal{B}'_{\boldsymbol{\omega}} := \mathcal{C}(D_1, \boldsymbol{\omega})$ with $\boldsymbol{\omega} \neq \mathbf{1}/N_1$ from which to sample M points $S'_1 \sim \mathcal{B}'^M_{\boldsymbol{\omega}}$. To make the model look fairer, the company needs the $\widehat{\Phi}_s$ computed with these cherry-picked points to have a small magnitude. The critical observation to motivate our approach is that the estimated GSV converges in probability to a **linear** function of the non-uniform weights.

Proposition 4.1. *Let S'_0 be **fixed**, and let $\xrightarrow{p}$ represent convergence in probability as the size M of the set $S'_1 \sim \mathcal{B}'^M_{\boldsymbol{\omega}}$ increases, we have*

$$\widehat{\Phi}_s(f, S'_0, S'_1) \xrightarrow{p} \sum_{\boldsymbol{z}^{(j)} \in D_1} \omega_j \, \widehat{\Phi}_s(f, S'_0, \boldsymbol{z}^{(j)}). \tag{9}$$

The proof is given in Appendix A.1.

We note that the coefficients $\widehat{\Phi}_s(f, S'_0, \boldsymbol{z}^{(j)})$ in Equation 9 are tractable and can be computed and stored by the company. We discuss in more detail how to compute them in Appendix B.3. Remember that to manipulate the GSV, the company must tune the weights $\boldsymbol{\omega}$ such that the explanation $\widehat{\Phi}_s$ is manipulated while ensuring that the non-uniform distribution $\mathcal{B}'_{\boldsymbol{\omega}}$ remains similar to the original $\mathcal{B}$. Otherwise, the fraud could be detected by the audit. Here the notion of similarity between distributions will be captured by the Wasserstein distance in output space.

Definition 4.1 (Wassertein Distance)**.** *Any probability measure π over $D_1 \times D_1$ is called a coupling measure between $\mathcal{B}$ and $\mathcal{B}'_{\boldsymbol{\omega}}$, denoted $\pi \in \Delta(\mathcal{B}, \mathcal{B}'_{\boldsymbol{\omega}})$, if $1/N_1 = \sum_j \pi_{ij}$ and $\omega_j = \sum_i \pi_{ij}$. The Wassertein distance between $\mathcal{B}$ and $\mathcal{B}'_{\boldsymbol{\omega}}$ mapped to the output-space is defined as*

$$\mathcal{W}(\mathcal{B}, \mathcal{B}'_{\boldsymbol{\omega}}) = \min_{\pi \in \Delta(\mathcal{B}, \mathcal{B}'_{\boldsymbol{\omega}})} \sum_{i,j} |f(\boldsymbol{z}^{(i)}) - f(\boldsymbol{z}^{(j)})| \pi_{ij}, \tag{10}$$

representing the cost of the optimal transport plan that distributes the probability mass from one distribution to the other.

We propose the Algorithm 1 to compute the non-uniform weights $\boldsymbol{\omega}$ by minimizing the magnitude of the GSV while maintaining a small Wasserstein distance. The trade-off between attribution manipulation and proximity to the data is tuned via a hyper-parameter $\lambda > 0$. We show in the Appendix A.2 that the optimization problem at line 5 of Algorithm 1 can be reformulated as a Minimum Cost Flow (MCF) and hence can be solved in polynomial time (more precisely $\widetilde{\mathcal{O}}(N_1^{2.5})$ as in Fukuchi et al. (2020)).

Algorithm 1 Compute non-uniform weights

1: **procedure** COMPUTE_WEIGHTS($D_1, \left\{\widehat{\Phi}_s(f, S'_0, \boldsymbol{z}^{(j)})\right\}_j, \lambda$)
2: $\quad \beta \;\; := \text{sign}[\sum_{\boldsymbol{z}^{(j)} \in D_1} \widehat{\Phi}_s(f, S'_0, \boldsymbol{z}^{(j)})\,]$
3: $\quad \mathcal{B} \;\; := \mathcal{C}(D_1, \mathbf{1}/N_1)$ ▷ Unmanipulated background
4: $\quad \mathcal{B}'_{\boldsymbol{\omega}} := \mathcal{C}(D_1, \boldsymbol{\omega})$ ▷ Manipulated background as a function of $\boldsymbol{\omega}$
5: $\quad \boldsymbol{\omega} = \arg\min_{\boldsymbol{\omega}} \;\; \beta \sum_{\boldsymbol{z}^{(j)} \in D_1} \omega_j \, \widehat{\Phi}_s(f, S'_0, \boldsymbol{z}^{(j)}) + \lambda \mathcal{W}(\mathcal{B}, \mathcal{B}'_{\boldsymbol{\omega}})$ ▷ Optimization Problem
6: $\quad$ **return** $\boldsymbol{\omega}$;

4.2 DETECTION

We now discuss ways the audit can detect manipulation of the sampling procedure. Recall that the audit has previously been given access to $f(D_1), f(D_0)$ representing the model outputs across all instances in the private dataset. The audit will then be provided sub-samples S'_1, S'_0 of D_1, D_0 on which they can compute the output of the model and compare with $f(D_1), f(D_0)$. To assess whether or not the sub-samples provided by the company were sampled uniformly at random, the audit has to conduct statistical tests. The null hypothesis of these tests will be that S'_1, S'_0 were sampled uniformly at random from D_1, D_0. The detection Algorithm 2 with significance α uses both the Kolmogorov-Smirnov and Wald tests with Bonferonni corrections (i.e. the $\alpha/4$ terms in the Algorithm). The Kolmogorov-Smirnov and Wald tests are discussed in more details in appendix C.

Algorithm 2 Detection with significance α

1: **procedure** DETECT_FRAUD($f(D_0), f(D_1), f(S'_0), f(S'_1), \alpha, M$)
2: $\quad$ **for** $i = 0, 1$ **do**
3: $\quad\quad f(S_i) \sim \mathcal{C}(f(D_i), \mathbf{1}/N_i)^M$ ▷ Subsample without cheating.
4: $\quad\quad$ p-value-KS $=$ KS$(\, f(S_i), f(S'_i)\,)$ ▷ KS test comparing $f(S_i)$ and $f(S'_i)$
5: $\quad\quad$ p-value-Wald $=$ Wald$(\, f(S'_i), f(D_i)\,)$ ▷ Wald test
6: $\quad\quad$ **if** p-value-KS $< \alpha/4$ **or** p-value-Wald $< \alpha/4$ **then** ▷ Reject the null hypothesis
7: $\quad\quad\quad$ **return** 1
8: $\quad$ **return** 0;

4.3 WHOLE PROCEDURE

The procedure returning the subsets S'_0, S'_1 is presented in Algorithm 3. It conducts a log-space search between λ_{min} and λ_{max} for the λ hyper-parameter (line 6) in order to explore the space of possible attacks. For each value of λ, the attacker runs Algorithm 1 to obtain $\mathcal{B}'_{\boldsymbol{\omega}}$ (line 7-8), then repeatedly samples $S'_1 \sim \mathcal{B}'^M_{\boldsymbol{\omega}}$ (line 11) and attempts to detect the fraud via the detection algorithm (line 12). The attacker will choose $\mathcal{B}'_{\boldsymbol{\omega}}$ that reduces the magnitude of $\widehat{\Phi}_s$ the most while having a detection rate below some threshold τ (line 14). An example of search over λ on a real-world dataset is presented in Figure 3. One of the limitations of the proposed methodology is that we only manipulate a single sensitive attribute. In appendix E.1, we present a possible extension of Algorithm 1 to handle multiple sensitive attributes and present preliminary results of its effectiveness.

4.4 CONTRIBUTIONS

We take a step back and clarify our specific contributions relative to the literature. The first study that manipulated `SHAP` with perturbations of the background distribution was conducted by Baniecki & Biecek (2022). They manipulated the background data given to `SHAP` via a genetic algorithm.

Algorithm 3 Fool SHAP

procedure FOOL_SHAP($f, D_0, D_1, M, \lambda_{\text{min}}, \lambda_{\text{max}}, \tau, \alpha$)
  $S'_0 \sim \mathcal{C}(D_0, \mathbf{1}/N_0)^M$ ▷ S'_0 is sampled without cheating
  Compute $\widehat{\Phi}_s(f, S'_0, \boldsymbol{z}^{(j)}) \quad \forall \boldsymbol{z}^{(j)} \in D_1$ ▷ cf. Section B.3
  $\mathcal{B}^\star = \mathcal{C}(D_1, \mathbf{1}/N_1)$
  $\Phi_s^\star = 1/N_1 \sum_{\boldsymbol{z}^{(j)} \in D_1} \widehat{\Phi}_s(f, S'_0, \boldsymbol{z}^{(j)})$ ▷ Initialize the solution
  for $\lambda = \lambda_{\text{min}}, \ldots, \lambda_{\text{max}}$ **do**
    $\boldsymbol{\omega} = \text{COMPUTE\_WEIGHTS}(D_1, \{\widehat{\Phi}_s(f, S'_0, \boldsymbol{z}^{(j)})\}_j, \lambda)$
    $\mathcal{B}'_{\boldsymbol{\omega}} = \mathcal{C}(D_1, \boldsymbol{\omega})$
    `Detection_rate` $= 0$
    for rep $= 1, \ldots, 100$ **do** ▷ Detect the manipulation
      $S'_1 \sim \mathcal{B}'^M_{\boldsymbol{\omega}}$
      `Detection_rate` += DETECT_FRAUD($f(D_0), f(D_1), f(S'_0), f(S'_1), \alpha, M$)
    if $|\sum_{\boldsymbol{z}^{(j)} \in D_1} \omega_j \widehat{\Phi}_s(f, S'_0, \boldsymbol{z}^{(j)})| < |\Phi_s^\star|$ **and** `Detection_rate` $< 100\tau$ **then**
      $\mathcal{B}^\star = \mathcal{B}'_{\boldsymbol{\omega}}$
      $\Phi_s^\star = \sum_{\boldsymbol{z}^{(j)} \in D_1} \omega_j \widehat{\Phi}_s(f, S'_0, \boldsymbol{z}^{(j)})$ ▷ Update the solution
  $S'_1 \sim \mathcal{B}^{\star M}$ ▷ Cherry-pick by sampling from the non-uniform background
  return S'_0, S'_1

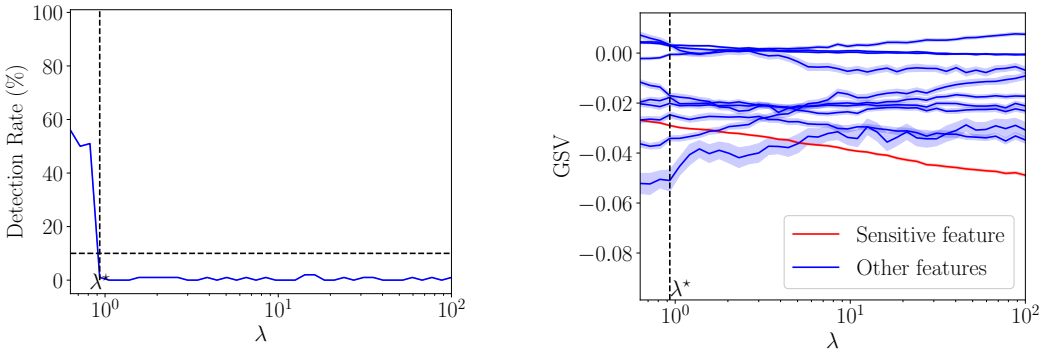

Figure 3: Example of log-space search over values of λ using a XGBoost classifier fitted on Adults. (a) The detection rate as a function of the parameter λ of the attack. The attacker uses a detection rate threshold $\tau = 10\%$. (b) For each value of λ, the vertical slice of the 11 curves is the GSV obtained with the resulting $\mathcal{B}'_{\boldsymbol{\omega}}$. The goal here is to reduce the amplitude of the sensitive feature (red curve) in order to hide its direct effect when explaining the disparity in model outcomes.

However, the objective did not consider that the manipulated background should remain "similar" to the original one. Our contribution is the addition of the Wasserstein distance with the objective to keep the modified background close to the original. A consequence of this addition is that an external audit can reproduce our fake feature attribution while being unable to detect that the background was modified. Since we rely on stealthily biased sampling, our approach is linked to the method of Fukuchi et al. (2020). Indeed, they use a similar MCF formulation to compute non-uniform weights over the empirical data distribution. Nonetheless, they focus on manipulating the fairness metric itself (*e.g.* reduce the Demographic Parity), while we perturb the `SHAP` feature attributions. In a sense, our approach is a generalization of their method to other problems. Since `SHAP` is a very popular tool for explaining black-box models, the fact that we can use stealthily-biased sampling almost directly for this purpose is the core finding of the current study. That is, no one was aware of the fact that such a strong malicious attack is possible so easily, without inventing completely new methods. We believe discovering the fact that such a malicious attack can be performed so easily while remaining undetectable is an important contribution to the field of *Explainable AI*.

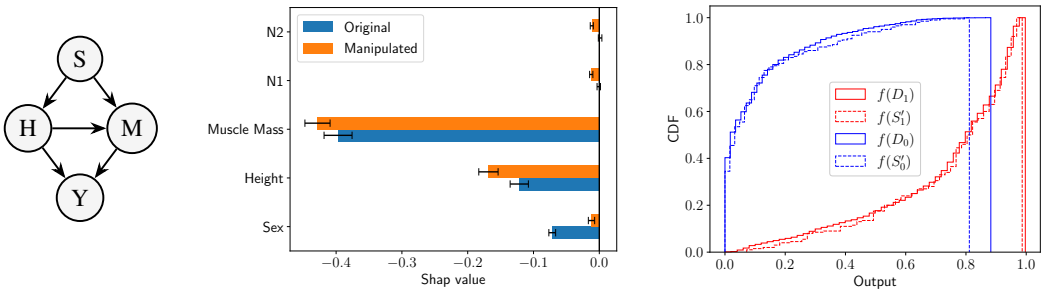

Figure 4: Toy example of hiring data for a job with specific physical requirements. Left: Causal graph. Middle: GSV before and after the attack with $M = 200$. Right: Comparison of the CDF of the misleading subsets $f(S'_0), f(S'_1)$ and the CDF over the whole data. $f(D_0), f(D_1)$. Here the audit is not able to detect the fraud using their detection algorithm.

5 Experiments

5.1 Toy experiment

We start with a toy example to illustrate the attack. The task is predicting whether an individual will be hired for a job that requires carrying heavy objects. The causal graph for this toy data is presented in Figure 4 (left). We observe that sex (S) influences height (H), and that both these features influence the Muscular Mass (M). In the end, the hiring decisions (Y) are only based on the two attributes relevant to the job: H and M. Also, two noise features $N1, N2$ were added. More details and justifications for this causal graph are discussed in Appendix D.1. Since strength and height (the two important qualifications for applicants) are correlated with sex, any model f that fits the data will exhibit some disparity in hiring rates between sexes. Although, if the decisions made by the model do not rely strongly on feature S, the company can argue in favor of deployment. GSVs are used by the audit to measure the amount by which the model relies on the sex feature, see Figure 4 (Middle). By manipulating `SHAP` with $M = 200$, the company is able to reduce the amplitude of the GSV of feature S. More importantly, the audit is not able to detect that the provided samples S'_0, S'_1 were cherry-picked, see Figure 4 (Right).

5.2 Datasets

Four real-world datasets were investigated, COMPAS, Adult-Income, Marketing, and Communities, which are often studied in the Fairness literature.

- **COMPAS** regroups 6,150 records from criminal offenders in Florida collected from 2013 and 2014. This binary classification task consists in predicting which individual will re-offend within two years. The sensitive feature s is `race` with values $x_s = 0$ for African-Americans and $x_s = 1$ for Caucasians.
- **Adult Income** contains demographic attributes of 48,842 individuals from the 1994 U.S. census. It is a binary classification problem with the goal of predicting whether or not a particular person makes more than 50K USD per year. The sensitive feature s in this dataset is `gender`, which took values $x_s = 0$ for female, and $x_s = 1$ for male.
- **Marketing** involves information of 41,175 customers of a Portuguese bank and the binary classification task is to predict who will subscribe to a term deposit. The sensitive attribute is `age` and took values $x_s = 0$ for age `30-60`, and $x_s = 1$ for age `not30-60`
- **Communities & Crime** contains per-capita violent crimes for 1994 different communities in the US. The binary classification task is to predict which communities have crimes below the median rate. The sensitive attribute is `PercentWhite` and took values $x_s = 0$ for `PercentWhite<90%`, and $x_s = 1$ for `PercentWhite>=90%`.

Three models were considered for the two datasets: Multi-Layered Perceptrons (MLP), Random Forests (RF), and eXtreme Gradient Boosted trees (XGB). One model of each type was fitted on each dataset for 5 different train/test splits seeds, resulting in 60 models total. Values of the test set

accuracy and demographic parity for each model type and dataset are presented in Appendix D.2. We note that all demographic parity values are negative.

5.3 Detector Calibration

Detector calibration refers to the assessment that, assuming the null hypothesis to be true, the probability of rejecting it (i.e. false positive) should be bounded by the significance level α. Remember that the null hypothesis is that the sets S_0', S_1' provided by the company are sampled uniformly from D_0, D_1. Hence, to test the detector, the audit can sample their own subsets $f(S_0), f(S_1)$ uniformly from $f(D_0), f(D_1)$, run the detection algorithm, and count the number of detection over 1000 repeats. Table 1 presents the probabilities of false positives over the five train-test splits using a significance level $\alpha = 1\%$. We observe that the probability of false positives is indeed bounded by α for all model types and datasets implying that the detector employed by the audit is calibrated.

Table 1: Probability of False Positives (%) by the detector i.e. the probability that S_0, S_1 are considered cherry-picked when they are not. All probabilities should be under 1%.

	mlp	rf	xgb
COMPAS	0.70	0.89	0.74
Adult	0.98	0.96	0.76
Marketing		0.80	0.94
Communities		0.72	0.88

5.4 Attack Results and Discussion

The first step of the attack (line 3 of Algorithm 3) requires that the company run `SHAP` on their own and compute the necessary coefficients to run Algorithm 1. For the COMPAS and Adults datasets, the `ExactExplainer` of `SHAP` was used. Since Marketing and Communities contain more than 15 features, and since the `ExactExplainer` scales exponentially with the number of features, we were restricted to using the `TreeExplainer` (Lundberg et al., 2020) on these datasets. The `TreeExplainer` avoids the exponential cost of Shapley values but is only applicable to tree-based models such as RFs and XGBs. Therefore, we could not conduct the attack on MLPs fitted on Marketing and Communities.

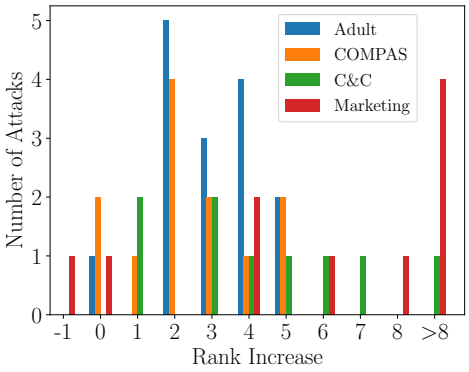

Figure 5: Increase in rank of the GSV $\widehat{\Phi}_s$ induced by the attack (i.e. $\text{rank}_{\text{after attack}} - \text{rank}_{\text{before attack}}$). Note that ranks consider the sign of the feature attribution hence a small rank (e.g. 1, 2) implies that the feature has the most negative effect on demographic parity. Increasing the rank of $\widehat{\Phi}_s$ means that the real negative effect of the sensitive attribute is being masked by other features.

The following step is to solve the MCF for various values of λ (line 7 of Algorithm 3). As stated previously, solving the MCF can be done in polynomial time in terms of N_1, which was tractable for a small dataset like COMPAS and Communities, but not for larger datasets like Adult and Marketing. To solve this issue, as was done in Fukuchi et al. (2020), we compute the manipulated weights multiple times using 5 bootstrap sub-samples of D_1 of size 2000 to obtain a set of weights $\boldsymbol{\omega}^{[1]}, \boldsymbol{\omega}^{[2]}, \ldots, \boldsymbol{\omega}^{[5]}$ which we average to obtain the final weights $\boldsymbol{\omega}$.

Results of 47 attacks with $M = 200$ are shown in Figure 5. Specific examples of the conducted attacks are presented in Appendix E.2. We note that in all runs but five, we are able to increase the rank of the GSV $\widehat{\Phi}_s$ hence masking the negative effect of the sensitive feature by other features. For the five attacks that could not increase the rank of the sensitive feature, we note that the amplitude of the attribution still diminished. Interestingly, the datasets Marketing and Communities, which have the most features, are the ones that exhibit the largest increases in ranks. This suggests that having more features leaves more "room" to lie about what features are really important. Such a hypothesis remains to be verified and is left as future work. Importantly, for every attack, the audit was unable to detect the fraud using statistical tests. This observation raises concerns about the risk that `SHAP` explanations can be attacked to return not only manipulated attributions but also non-detectable fake evidence of fairness.

6 CONCLUSION

To conclude, we proposed a novel attack on Shapley values that does not require modifying the model but rather manipulates the sampling procedure that estimates expectations w.r.t the background distributions. We show on a toy example and four fairness datasets that our attack can reduce the importance of a sensitive feature when explaining the difference in outcomes between groups using `SHAP`. Moreover, the sampling manipulation is hard to detect by an audit that is given limited access to the data and model. These results raise concerns about the viability of using Shapley values to assess model fairness. We leave as future work the use of Shapley values to decompose other fairness metrics such as predictive equality and equal opportunity. Moreover, we wish to move to use cases beyond fairness, as we believe that the vulnerability of Shapley values that was demonstrated can apply to many other properties such as safety and security.

7 ETHICS STATEMENT

The main objective of this work is to raise awareness about the risk of manipulation of SHAP explanations and their undetectability. As such, it aims at exposing the potential negative societal impacts of relying on such explanations. It remains however possible that malicious model producers could use this attack to mislead end users or cheat during an audit. However, we believe this paper makes a significant step toward increasing the vigilance of the community and fostering the development of trustworthy explanations methods.

8 REPRODUCIBILITY STATEMENT

The source code of all experiments is available online[2]. Moreover, experimental details are provided in appendix D.2 for the interested reader.

REFERENCES

Julius A Adebayo et al. Fairml: Toolbox for diagnosing bias in predictive modeling. Master's thesis, Massachusetts Institute of Technology, 2016. 1

Ulrich Aïvodji, Hiromi Arai, Olivier Fortineau, Sébastien Gambs, Satoshi Hara, and Alain Tapp. Fairwashing: the risk of rationalization. In *International Conference on Machine Learning*, pp. 161–170. PMLR, 2019. 1

Hubert Baniecki and Przemyslaw Biecek. Manipulating shap via adversarial data perturbations (student abstract). 2022. 1, 6

Hubert Baniecki, Wojciech Kretowicz, and Przemyslaw Biecek. Fooling partial dependence via data poisoning. *arXiv preprint arXiv:2105.12837*, 2021. 1

Tom Begley, Tobias Schwedes, Christopher Frye, and Ilya Feige. Explainability for fair machine learning. *arXiv preprint arXiv:2010.07389*, 2020. 1, 3

Rachel KE Bellamy, Kuntal Dey, Michael Hind, Samuel C Hoffman, Stephanie Houde, Kalapriya Kannan, Pranay Lohia, Jacquelyn Martino, Sameep Mehta, Aleksandra Mojsilovic, et al. Ai fairness 360: An extensible toolkit for detecting, understanding, and mitigating unwanted algorithmic bias. *arXiv preprint arXiv:1810.01943*, 2018. 1

Yoichi Chikahara, Shinsaku Sakaue, Akinori Fujino, and Hisashi Kashima. Learning individually fair classifier with path-specific causal-effect constraint. In *International Conference on Artificial Intelligence and Statistics*, pp. 145–153. PMLR, 2021. 1

Sam Corbett-Davies, Emma Pierson, Avi Feller, Sharad Goel, and Aziz Huq. Algorithmic decision making and the cost of fairness. In *Proceedings of the 23rd acm sigkdd international conference on knowledge discovery and data mining*, pp. 797–806, 2017. 4

[2] `https://github.com/gablabc/Fool_SHAP`

Botty Dimanov, Umang Bhatt, Mateja Jamnik, and Adrian Weller. You shouldn't trust me: Learning models which conceal unfairness from multiple explanation methods. In *SafeAI@ AAAI*, 2020. 1

Cynthia Dwork, Moritz Hardt, Toniann Pitassi, Omer Reingold, and Richard Zemel. Fairness through awareness. In *Proceedings of the 3rd innovations in theoretical computer science conference*, pp. 214–226, 2012. 4

Kazuto Fukuchi, Satoshi Hara, and Takanori Maehara. Faking fairness via stealthily biased sampling. In *Proceedings of the AAAI Conference on Artificial Intelligence*, volume 34, pp. 412–419, 2020. 1, 2, 6, 7, 9

Riccardo Guidotti, Anna Monreale, Salvatore Ruggieri, Franco Turini, Fosca Giannotti, and Dino Pedreschi. A survey of methods for explaining black box models. *ACM computing surveys (CSUR)*, 51(5):1–42, 2018. 1

Moritz Hardt, Eric Price, and Nati Srebro. Equality of opportunity in supervised learning. *Advances in neural information processing systems*, 29, 2016. 4

Ian Janssen, Steven B Heymsfield, ZiMian Wang, and Robert Ross. Skeletal muscle mass and distribution in 468 men and women aged 18–88 yr. *Journal of applied physiology*, 2000. 20

A J Lee. *U-statistics: Theory and Practice*. Routledge, 2019. 18

Scott M Lundberg and Su-In Lee. A unified approach to interpreting model predictions. *Advances in neural information processing systems*, 30, 2017. 1, 2

Scott M Lundberg, Gabriel Erion, Hugh Chen, Alex DeGrave, Jordan M Prutkin, Bala Nair, Ronit Katz, Jonathan Himmelfarb, Nisha Bansal, and Su-In Lee. From local explanations to global understanding with explainable ai for trees. *Nature machine intelligence*, 2(1):56–67, 2020. 9, 17

Frank J Massey Jr. The kolmogorov-smirnov test for goodness of fit. *Journal of the American statistical Association*, 46(253):68–78, 1951. 19

Pedro Saleiro, Benedict Kuester, Loren Hinkson, Jesse London, Abby Stevens, Ari Anisfeld, Kit T Rodolfa, and Rayid Ghani. Aequitas: A bias and fairness audit toolkit. *arXiv preprint arXiv:1811.05577*, 2018. 1

Lloyd S Shapley. A value for n-person games. *Contributions to the Theory of Games*, pp. 307–317, 1953. 2

Dylan Slack, Sophie Hilgard, Emily Jia, Sameer Singh, and Himabindu Lakkaraju. Fooling lime and shap: Adversarial attacks on post hoc explanation methods. In *Proceedings of the AAAI/ACM Conference on AI, Ethics, and Society*, pp. 180–186, 2020. 1

Larry Wasserman. *All of Statistics: A concise course in statistical inference*. Springer, 2004. 13

A PROOFS

A.1 PROOFS FOR GSV

Proposition A.1 (**Proposition 2.1**). *The GSV have the following property*

$$\sum_{i=1}^{d} \Phi_i(f, \mathcal{F}, \mathcal{B}) = \mathop{\mathbb{E}}_{\boldsymbol{x}\sim\mathcal{F}}[f(\boldsymbol{x})] - \mathop{\mathbb{E}}_{\boldsymbol{x}\sim\mathcal{B}}[f(\boldsymbol{x})]. \tag{11}$$

Proof. As a reminder, we have defined the vector

$$\boldsymbol{\Phi}(f, \mathcal{F}, \mathcal{B}) = \mathop{\mathbb{E}}_{\substack{\boldsymbol{x}\sim\mathcal{F}\\ \boldsymbol{z}\sim\mathcal{B}}}\big[\boldsymbol{\phi}(f, \boldsymbol{x}, \boldsymbol{z})\big], \tag{12}$$

whose components sum up to

$$\begin{aligned}
\sum_{i=1}^{d} \Phi_i(f, \mathcal{F}, \mathcal{B}) &= \sum_{i=1}^{d} \mathop{\mathbb{E}}_{\substack{\boldsymbol{x}\sim\mathcal{F}\\ \boldsymbol{z}\sim\mathcal{B}}}[\,\phi_i(f, \boldsymbol{x}, \boldsymbol{z})\,] && (13)\\
&= \mathop{\mathbb{E}}_{\substack{\boldsymbol{x}\sim\mathcal{F}\\ \boldsymbol{z}\sim\mathcal{B}}}\left[\sum_{i=1}^{d} \phi_i(f, \boldsymbol{x}, \boldsymbol{z})\right] && (14)\\
&= \mathop{\mathbb{E}}_{\substack{\boldsymbol{x}\sim\mathcal{F}\\ \boldsymbol{z}\sim\mathcal{B}}}[\,f(\boldsymbol{x}) - f(\boldsymbol{z})\,] && (15)\\
&= \mathop{\mathbb{E}}_{\boldsymbol{x}\sim\mathcal{F}}[f(\boldsymbol{x})] - \mathop{\mathbb{E}}_{\boldsymbol{z}\sim\mathcal{B}}[f(\boldsymbol{z})] && (16)\\
&= \mathop{\mathbb{E}}_{\boldsymbol{x}\sim\mathcal{F}}[f(\boldsymbol{x})] - \mathop{\mathbb{E}}_{\boldsymbol{x}\sim\mathcal{B}}[f(\boldsymbol{x})], && (17)
\end{aligned}$$

where at the last step we have simply renamed a dummy variable. □

Proposition A.2 (**Proposition 4.1**). *Let S'_0 be **fixed**, and let $\xrightarrow{p}$ represent convergence in probability as the size M of the set $S'_1 \sim \mathcal{B}'^M$ increases, we have*

$$\widehat{\Phi}_s(f, S'_0, S'_1) \xrightarrow{p} \sum_{j=1}^{N_1} \omega_j\, \widehat{\Phi}_s(f, S'_0, \boldsymbol{z}^{(j)}). \tag{18}$$

Proof.

$$\begin{aligned}
\widehat{\boldsymbol{\Phi}}(f, S'_0, S'_1) &= \frac{1}{M^2} \sum_{\boldsymbol{x}^{(i)}\in S'_0} \sum_{\boldsymbol{z}^{(j)}\in S'_1} \boldsymbol{\phi}(f, \boldsymbol{x}^{(i)}, \boldsymbol{z}^{(j)})\\
&= \frac{1}{M} \sum_{\boldsymbol{z}^{(j)}\in S'_1} \left(\frac{1}{M} \sum_{\boldsymbol{x}^{(i)}\in S'_0} \boldsymbol{\phi}(f, \boldsymbol{x}^{(i)}, \boldsymbol{z}^{(j)})\right) && (19)\\
&= \frac{1}{M} \sum_{\boldsymbol{z}^{(j)}\in S'_1} \widehat{\boldsymbol{\Phi}}(f, S'_0, \boldsymbol{z}^{(j)}).
\end{aligned}$$

Since S'_0 is assumed to be fixed, then the only random variable in $\widehat{\Phi}_s(f, S'_0, \boldsymbol{z}^{(j)})$ is $\boldsymbol{z}^{(j)}$ which represents an instance sampled from the $\mathcal{B}'$. Therefore, we can define $\psi(\boldsymbol{z}) := \widehat{\Phi}_s(f, S'_0, \boldsymbol{z})$ and we get

$$\begin{aligned}
\widehat{\Phi}_s(f, S'_0, S'_1) &= \frac{1}{M} \sum_{\boldsymbol{z}^{(j)}\in S'_1} \widehat{\Phi}_s(f, S'_0, \boldsymbol{z}^{(j)})\\
&= \frac{1}{M} \sum_{\boldsymbol{z}^{(j)}\in S'_1} \psi(\boldsymbol{z}^{(j)}) \qquad \text{with } S'_1 \sim \mathcal{B}'^M. && (20)
\end{aligned}$$

By the weak law of large number, the following holds as M goes to infinity (Wasserman, 2004, Theorem 5.6)

$$\frac{1}{M}\sum_{\boldsymbol{z}^{(j)}\in S_1'}\psi(\boldsymbol{z}^{(j)}) \xrightarrow{p} \mathop{\mathbb{E}}_{\boldsymbol{z}\sim\mathcal{B}'}[\psi(\boldsymbol{z})]. \tag{21}$$

Now, as a reminder, the manipulated background distribution is $\mathcal{B}' := \mathcal{C}(D_1, \boldsymbol{\omega})$ with $\boldsymbol{\omega} \neq \mathbf{1}/N_1$. Therefore

$$\begin{aligned}\widehat{\Phi}_s(f, S_0', S_1') &\xrightarrow{p} \mathop{\mathbb{E}}_{\boldsymbol{z}\sim\mathcal{B}'}[\psi(\boldsymbol{z})] \\ &= \mathop{\mathbb{E}}_{\boldsymbol{z}\sim\mathcal{C}(D_1,\boldsymbol{\omega})}[\psi(\boldsymbol{z})] \\ &= \sum_{j=1}^{N_1}\omega_j\psi(\boldsymbol{z}^{(j)}) \\ &= \sum_{j=1}^{N_1}\omega_j\widehat{\Phi}_s(f, S_0', \boldsymbol{z}^{(j)})\end{aligned} \tag{22}$$

concluding the proof. □

A.2 Proofs for Optimization Problem

A.2.1 Technical Lemmas

We provide some technical lemmas that will be essential when proving Theorem A.1. These lemmas and proofs are provided here for completeness and are not meant as contributions by the authors.

Let us first write the formal definition of the minimum of a function.

Definition A.1 (Minimum)**.** *Given some function $f : D \to \mathbb{R}$, the minimum of f over D (denoted $f^\star$) is defined as follows:*

$$f^\star = \min_{x\in D} f(x) \iff \exists x^\star \in D \text{ s.t. } f^\star = f(x^\star) \leqslant f(x) \quad \forall x \in D.$$

Basically, the notion of minimum coincides with the notion of infimum (highest lower bound) of $f(D)$ when this lower bound is attained for some $x^\star \in D$. For the rest of this appendix, we shall only study constrained optimization problems where points from the feasible set $D = \{(x, y) : x \in \mathcal{X}, y \in \mathcal{Y}_x \subset \mathcal{Y}\}$ can be *selected* by the following procedure

1. Choose some $x \in \mathcal{X}$
2. Given the selected x, choose some $y \in \mathcal{Y}_x \subset \mathcal{Y}$ where the set $\mathcal{Y}_x$ is non-empty and depends on the value of x.

When optimizing objective functions over these types of domains, one can optimize in two steps as highlighted in the following lemma.

Lemma A.1. *Given a feasible set D of the form described above and an objective function $f : \mathcal{X} \times \mathcal{Y} \to \mathbb{R}$, the following holds*

$$\min_{(x,y)\in D} f(x, y) = \min_{x\in\mathcal{X}}\min_{y\in\mathcal{Y}_x} f(x, y).$$

Proof. Let $\widetilde{f}(x) := \min_{y\in\mathcal{Y}_x} f(x, y)$, which is a well defined function on $\mathcal{X}$ since $\mathcal{Y}_x$ is non-empty for any $x \in \mathcal{X}$. By the definition of the minimum, we have

$$\forall x \in \mathcal{X},\ \exists y^\star(x) \in \mathcal{Y}_x \quad \text{s.t.} \quad \widetilde{f}(x) = f(x, y^\star(x)) \leqslant f(x, y) \quad \forall y \in \mathcal{Y}_x. \tag{23}$$

Now, we can optimize $\widetilde{f}$ with respect to x i.e. $f^\star = \min_{x\in\mathcal{X}} \widetilde{f}(x)$. By applying once again the definition of the minimum, we get

$$\exists x^\star \in \mathcal{X} \quad \text{s.t.} \quad f^\star = \widetilde{f}(x^\star) \leqslant \widetilde{f}(x) \quad \forall x \in \mathcal{X}. \tag{24}$$

By virtue of Equation 23, we have that $\widetilde{f}(x^\star) = f(x^\star, y^\star(x^\star)) = f(x^\star, y^\star)$, where we labeled $y^\star := y^\star(x^\star)$ for convenience. We get

$$\begin{aligned} \exists (x^\star, y^\star) \in D \quad \text{s.t.} \quad f(x^\star, y^\star) &\leqslant f(x, y^\star(x)) \quad \forall\, x \in \mathcal{X} && \text{(cf. Equation 24)} \\ &\leqslant f(x, y) \qquad \forall\, y \in \mathcal{Y}_x. && \text{(cf. Equation 23)} \end{aligned}$$

Hence we have proven that $\exists (x^\star, y^\star) \in D \quad \text{s.t.} \quad f(x^\star, y^\star) \leqslant f(x, y) \;\; \forall (x, y) \in D$, which concludes the proof. □

Lemma A.2. *Given a feasible set D of the form described above and two functions $h : \mathcal{X} \to \mathbb{R}$ and $g : \mathcal{Y} \to \mathbb{R}$, then*

$$\min_{(x,y)\in D} \Big(h(x) + g(y) \Big) = \min_{x \in \mathcal{X}} \Big(h(x) + \min_{y \in \mathcal{Y}_x} g(y) \Big)$$

Proof. Applying Lemma A.1 with the function $f(x, y) := h(x) + g(y)$ leads to the desired result. □

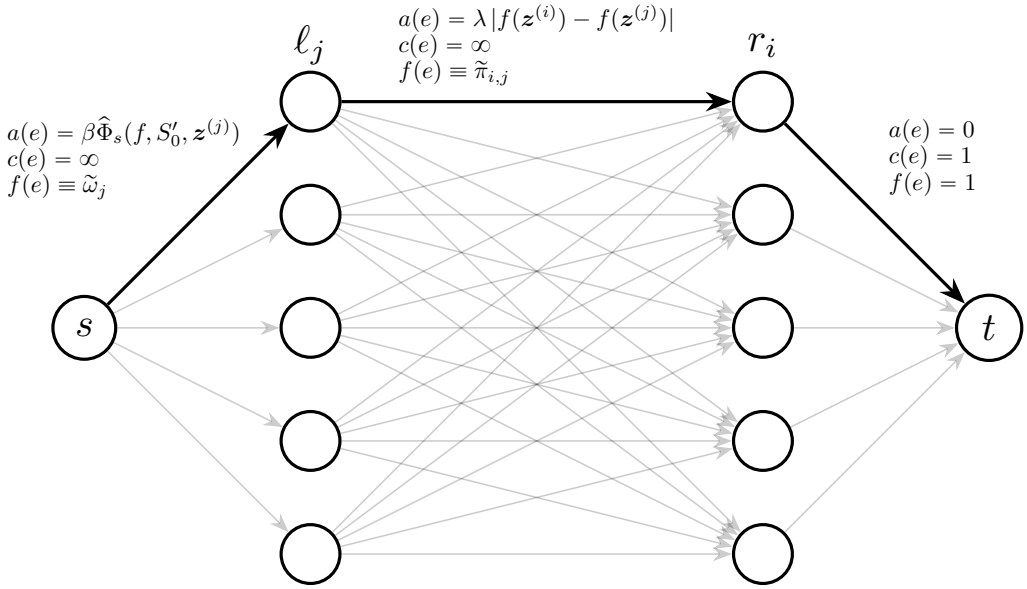

Figure 6: Graph $\mathbb{G}$ on which we solve the MCF. Note that the total amount of flow is $d = N_1$ and there are N_1 left and right nodes ℓ_j, r_i.

A.2.2 Minimum Cost Flows

Let $\mathbb{G} = (\mathcal{V}, \mathcal{E})$ be a graph with vertices $v \in \mathcal{V}$ with directed edges $e \in \mathcal{E} \subset \mathcal{V} \times \mathcal{V}$, $c : \mathcal{E} \to \mathbb{R}^+$ be a capacity and $a : \mathcal{E} \to \mathbb{R}$ be a cost. Moreover, let $s, t \in \mathcal{E}$ be two special vertices called the source and the sink respectivelly, and $d \in \mathbb{R}^+$ be a total flow. The Minimum-Cost Flow (MCF) problem of $\mathbb{G}$ consists of finding the flow function $f : \mathcal{E} \to \mathbb{R}^+$ that minimizes the total cost

$$\begin{aligned} \min_f \quad & \sum_{e \in \mathcal{E}} a(e) f(e) \\ \text{s.t.} \quad & 0 \leqslant f(e) \leqslant c(e) \;\; \forall e \in \mathcal{E} \\ & \sum_{e \in u^+} f(e) - \sum_{e \in u^-} f(e) = \begin{cases} 0 & u \in \mathcal{V} \setminus \{s, t\} \\ d & u = s \\ -d & u = t \end{cases} \end{aligned} \tag{25}$$

where $u^+ := \{(u, v) \in \mathcal{E}\}$ and $u^- := \{(v, u) \in \mathcal{E}\}$ are the outgoing and incoming edges from u. The terminology of *flow* arises from the constraint that, for vertices that are not the source nor the sink, the outgoing flow must equal the incoming one, which is reminiscent of conservation laws in fluidic. We shall refer to $f((u, v))$ as the flow from u to v.

Now that we have introduced minimum cost flows, let us specify the graph that will be employed to manipulate GSV, see Figure 6. We label the flow going from the sink s to one of the left vertices as $\widetilde{\omega}_i \equiv \omega_i \times N_1$, and the flow going from ℓ_j to r_i as $\widetilde{\pi}_{i,j} \equiv \pi_{i,j} \times N_1$. The required flow is fixed at $d = N_1$.

Theorem A.1. *Solving the MCF of Figure 6 leads to a solution of the linear program in Algorithm 1.*

Proof. We begin by showing that the flow conservation constraints in the MCF imply that π is a coupling measure (i.e. $\pi \in \Delta(\mathcal{B}, \mathcal{B}')$), and $\boldsymbol{\omega}$ is constrained to the probability simplex $\Delta(N_1)$. Applying the conservation law on the left-side of the graph leads to the conclusion that the flows entering vertices ℓ_j must sum up to N_1

$$\sum_{j=1}^{N_1} \widetilde{\omega}_j = N_1.$$

This implies that $\boldsymbol{\omega}$ is must be part of the probability simplex. By conservation, the amount of flow that leaves a specific vertex ℓ_j must also be $\widetilde{\omega}_j$, hence

$$\sum_i \widetilde{\pi}_{ij} = \widetilde{\omega}_j.$$

For any edge outgoing from r_i to the sink t, the flow must be exactly 1. This is because we have N_1 edges with capacity $c(e) = 1$ going into the sink and the sink must receive an incoming flow of N_1. As a consequence of the conservation law on a specific vertex r_i, the amount of flow that goes into each r_i is also 1

$$\sum_j \widetilde{\pi}_{ij} = 1.$$

Putting everything together, from the conservation laws on $\mathbb{G}$, we have that $\boldsymbol{\omega} \in \Delta(N_1)$, and $\pi \in \Delta(\mathcal{B}, \mathcal{B}')$.

Now, to make the parallel between the MCF and Algorithm 1, we must use Lemma A.2. As a reminder, the Lemma states that for specific types of domains, one can solve the constrained optimization problem in two optimization steps. Note that $\boldsymbol{\omega}$ is restricted to the probability simplex, while π is restricted to be a coupling measure. Importantly, the set of all possible coupling measures $\Delta(\mathcal{B}, \mathcal{B}')$ is different for each $\boldsymbol{\omega}$ (and non-empty) because $\mathcal{B}'$ depends on $\boldsymbol{\omega}$. Hence, we study a feasible set with the same structure as the ones tackled in the Lemma A.2 (where $x \in \mathcal{X}$ becomes $\boldsymbol{\omega} \in \Delta(N_1)$) and $y \in \mathcal{Y}_x$ becomes $\pi \in \Delta(\mathcal{B}, \mathcal{B}')$) and we can apply the Lemma A.2 to the objective function of the MCF.

$$\begin{aligned}
\min_f \sum_{e \in \mathcal{E}} f(e)a(e) &= \min_{\widetilde{\omega}, \widetilde{\pi}} \sum_{j=1}^{N_1} \beta \widetilde{\omega}_j \widehat{\Phi}_s(f, S_0', \boldsymbol{z}^{(j)}) + \lambda \sum_{i,j} \widetilde{\pi}_{ij} |f(\boldsymbol{z}^{(i)}) - f(\boldsymbol{z}^{(j)})| \\
&= \min_{\widetilde{\omega}, \widetilde{\pi}} \frac{N_1}{N_1} \left(\beta \sum_{j=1}^{N_1} \widetilde{\omega}_j \widehat{\Phi}_s(f, S_0', \boldsymbol{z}^{(j)}) + \lambda \sum_{i,j} \widetilde{\pi}_{ij} |f(\boldsymbol{z}^{(i)}) - f(\boldsymbol{z}^{(j)})| \right) \\
&= N_1 \min_{\widetilde{\omega}, \widetilde{\pi}} \left(\beta \sum_{j=1}^{N_1} \frac{\widetilde{\omega}_j}{N_1} \widehat{\Phi}_s(f, S_0', \boldsymbol{z}^{(j)}) + \lambda \sum_{i,j} \frac{\widetilde{\pi}_{ij}}{N_1} |f(\boldsymbol{z}^{(i)}) - f(\boldsymbol{z}^{(j)})| \right) \\
&= N_1 \min_{\boldsymbol{\omega} \in \Delta(N_1), \pi \in \Delta(\mathcal{B}, \mathcal{B}')} \left(\beta \sum_{j=1}^{N_1} \omega_j \widehat{\Phi}_s(f, S_0', \boldsymbol{z}^{(j)}) + \lambda \sum_{i,j} \pi_{i,j} |f(\boldsymbol{z}^{(i)}) - f(\boldsymbol{z}^{(j)})| \right) \\
&= N_1 \min_{\boldsymbol{\omega} \in \Delta(N_1), \pi \in \Delta(\mathcal{B}, \mathcal{B}')} \Big(h(\omega) + g(\pi) \Big) \\
&= N_1 \min_{\boldsymbol{\omega} \in \Delta(N_1)} \Big(h(\omega) + \min_{\pi \in \Delta(\mathcal{B}, \mathcal{B}')} g(\pi) \Big) \qquad \text{(cf Lemma A.2)} \\
&= N_1 \min_{\boldsymbol{\omega} \in \Delta(N_1)} \left(\beta \sum_{j=1}^{N_1} \omega_j \widehat{\Phi}_s(f, S_0', \boldsymbol{z}^{(j)}) + \lambda \min_{\pi \in \Delta(\mathcal{B}, \mathcal{B}')} \sum_{i,j} \pi_{i,j} |f(\boldsymbol{z}^{(i)}) - f(\boldsymbol{z}^{(j)})| \right) \\
&= N_1 \min_{\boldsymbol{\omega} \in \Delta(N_1)} \left(\beta \sum_{j=1}^{N_1} \omega_j \widehat{\Phi}_s(f, S_0', \boldsymbol{z}^{(j)}) + \lambda \, \mathcal{W}(\mathcal{B}, \mathcal{B}'_{\boldsymbol{\omega}}) \right)
\end{aligned}$$

which (up to a multiplicative constant N_1) is a solution of the linear program of Algorithm 1. □

B SHAPLEY VALUES

B.1 LOCAL SHAPLEY VALUES

We introduce Local Shapley Values (LSV) more formally. First of, as explained earlier, Shapley values are based on coalitional game theory where the different features work together toward a common outcome $f(\boldsymbol{x})$. In a game, the features can either be present or absent, which is simulated by replacing some features by a baseline value $\boldsymbol{z}$.

Definition B.1 (Replace Function)**.** *Given an input of interest $\boldsymbol{x}$, a subset of features $S \subseteq \{1, 2, \dots, d\}$ that are considered active, and a baseline input $\boldsymbol{z}$, the replace-function $\boldsymbol{r}_S : \mathbb{R}^d \times \mathbb{R}^d \to \mathbb{R}^d$ is defined as*

$$r_S(\boldsymbol{z}, \boldsymbol{x})_i = \begin{cases} x_i & \text{if } i \in S \\ z_i & \text{otherwise.} \end{cases} \tag{26}$$

We note that this function is meant to "activate" the features in S.

Now, if we let π be a random permutation of d features, and π_i denote all features that appear before i in π, the LSV are computed via

$$\phi_i(f, \boldsymbol{x}, \boldsymbol{z}) := \mathop{\mathbb{E}}_{\pi \sim \Omega} \big[f(\, \boldsymbol{r}_{\pi_i \cup \{i\}}(\boldsymbol{z}, \boldsymbol{x})\,) - f(\, \boldsymbol{r}_{\pi_i}(\boldsymbol{z}, \boldsymbol{x})\,) \big], \quad i = 1, 2, \dots, d, \tag{27}$$

where Ω is the uniform distribution over 2^d permutations. Observe that the computation of LSV is exponential w.r.t the number of features d hence model-agnostic computations are only possible with datasets with few features such as COMPAS and Adult-Income. For datasets with larger amounts of features the `TreeExplainer` algorithm (Lundberg et al., 2020) can be used to compute the LSV (cf. Equation 27) in polynomial time given that one is explaining a tree-based model.

B.2 CONVERGENCE

As a reminder, we are interested in estimating the GSV $\boldsymbol{\Phi} \equiv \boldsymbol{\Phi}(f, \mathcal{F}, \mathcal{B})$ which requires estimating expectations w.r.t the foreground and background distributions. Said estimations can be conducted with Monte-Carlo where we sample M instances

$$S_0 \sim \mathcal{F}^M \qquad S_1 \sim \mathcal{B}^M, \tag{28}$$

and compute the plug-in estimates

$$\begin{aligned} \widehat{\boldsymbol{\Phi}}(f, S_0, S_1) &:= \boldsymbol{\Phi}(f,\, \mathcal{C}(S_0, \mathbf{1}/M),\, \mathcal{C}(S_1, \mathbf{1}/M)) \\ &= \frac{1}{M^2} \sum_{\boldsymbol{x}^{(i)} \in S_0} \sum_{\boldsymbol{z}^{(j)} \in S_1} \boldsymbol{\phi}(f, \boldsymbol{x}^{(i)}, \boldsymbol{z}^{(j)}). \end{aligned} \tag{29}$$

We now show that, $\widehat{\boldsymbol{\Phi}}(f, S_0, S_1)$ is a consistent and asymptotically normal estimate of $\boldsymbol{\Phi}(f, \mathcal{F}, \mathcal{B})$

Proposition B.1. *Let $f : \mathcal{X} \to [0, 1]$ be a black box, $\mathcal{F}$ and $\mathcal{B}$ be distributions on $\mathcal{X}$, and $\widehat{\boldsymbol{\Phi}} \equiv \widehat{\boldsymbol{\Phi}}(f, S_0, S_1)$ be the plug-in estimate of $\boldsymbol{\Phi} \equiv \boldsymbol{\Phi}(f, \mathcal{F}, \mathcal{B})$, the following holds for any $\delta \in \,]0, 1[$ and $k = 1, 2 \dots, d$*

$$\lim_{M \to \infty} \mathbb{P}\left(|\widehat{\Phi}_k - \Phi_k| \geqslant \frac{F^{-1}_{\mathcal{N}(0,1)}(1 - \delta/2)}{2\sqrt{M}} \sqrt{\sigma^2_{10} + \sigma^2_{01}} \right) = \delta,$$

where $F^{-1}_{\mathcal{N}(0,1)}$ is the inverse Cumulative Distribution Function (CDF) of the standard normal distribution, $\sigma^2_{10} = \mathbb{V}_{\boldsymbol{x} \sim \mathcal{F}}[\, \mathbb{E}_{\boldsymbol{z} \sim \mathcal{B}}[\phi_i(f, \boldsymbol{x}, \boldsymbol{z}))]\,]$ and $\sigma^2_{01} = \mathbb{V}_{\boldsymbol{z} \sim \mathcal{B}}[\, \mathbb{E}_{\boldsymbol{x} \sim \mathcal{F}}[\phi_i(f, \boldsymbol{x}, \boldsymbol{z}))]\,]$.

Proof. The proof consists simply in noting that LSV $\phi_k(f, \boldsymbol{x}^{(i)}, \boldsymbol{z}^{(j)})$ are a function of two independent samples $\boldsymbol{x}^{(i)} \sim \mathcal{F}$ and $\boldsymbol{z}^{(j)} \sim \mathcal{B}$. The model f is assumed fixed and hence for any feature k we can define $h(\boldsymbol{x}^{(i)}, \boldsymbol{z}^{(j)}) := \phi_k(f, \boldsymbol{x}^{(i)}, \boldsymbol{z}^{(j)})$. Now, the estimates of GSV can be rewritten

$$\widehat{\Phi}_k(f, S_0, S_1) = \frac{1}{|S_0|\,|S_1|} \sum_{\boldsymbol{x}^{(i)} \in S_0} \sum_{\boldsymbol{z}^{(j)} \in S_1} h(\boldsymbol{x}^{(i)}, \boldsymbol{z}^{(j)}), \tag{30}$$

which we recognize as a well-known class of statistics called two-samples U-statistics. Such statistics are unbiased and asymptotically normal estimates of

$$\Phi_k(f, \mathcal{F}, \mathcal{B}) = \mathop{\mathbb{E}}_{\substack{\boldsymbol{x}\sim\mathcal{F}\\ \boldsymbol{z}\sim\mathcal{B}}}[h(\boldsymbol{x}, \boldsymbol{z})]. \tag{31}$$

The asymptotic normality of two-samples U-statistics is characterized by the following Theorem (Lee, 2019, Section 3.7.1).

Theorem B.1. *Let $\widehat{\Phi}_k \equiv \widehat{\Phi}_k(f, S_0, S_1)$ be a two-samples U-statistic with $|S_0| = N, |S_1| = M$, moreover let $h(\boldsymbol{x}, \boldsymbol{z})$ have finite first and second moments, then the following holds for any $\delta \in]0, 1[$*

$$\lim_{\substack{N+M\to\infty\\ \text{s.t. } N/(N+M)\to p\in(0,1)}} \mathbb{P}\left(|\widehat{\Phi}_k - \Phi_k| \geqslant \frac{F^{-1}_{\mathcal{N}(0,1)}(1-\delta/2)}{\sqrt{M+N}} \sqrt{\frac{\sigma^2_{10}}{p} + \frac{\sigma^2_{01}}{1-p}} \right) = \delta,$$

where $\sigma^2_{10} = \mathbb{V}_{\boldsymbol{x}\sim\mathcal{F}}[\,\mathbb{E}_{\boldsymbol{z}\sim\mathcal{B}}[h(\boldsymbol{x}, \boldsymbol{z})]\,]$ and $\sigma^2_{01} = \mathbb{V}_{\boldsymbol{z}\sim\mathcal{B}}[\,\mathbb{E}_{\boldsymbol{x}\sim\mathcal{F}}[h(\boldsymbol{x}, \boldsymbol{z})]\,]$.

Proposition B.1 follows from this Theorem by choosing $N = M, p = 0.5$ and noticing that having a model with bounded outputs ($f : \mathcal{X} \to [0, 1]$) implies that $|h(\boldsymbol{x}, \boldsymbol{z})| \leqslant 1\ \forall \boldsymbol{x}, \boldsymbol{z} \in \mathcal{X}$ which means that $h(\boldsymbol{x}, \boldsymbol{z})$ has bounded first and second moments. □

B.3 Compute the LSV

Running Algorithm 1 requires computing the coefficients $\widehat{\Phi}_s(f, S'_0, \boldsymbol{z}^{(j)})$ for $j = 1, 2, \ldots, N_1$. To compute them, first note that they can be written in terms of LSV for all instances in S'_0

$$\widehat{\Phi}_s(f, S'_0, \boldsymbol{z}^{(j)}) = \frac{1}{M} \sum_{\boldsymbol{x}^{(i)}\in S'_0} \phi_s(f, \boldsymbol{x}^{(i)}, \boldsymbol{z}^{(j)}). \tag{32}$$

The LSV $\phi_s(f, \boldsymbol{x}^{(i)}, \boldsymbol{z}^{(j)})$ are computed deeply in the `SHAP` code and are not directly accessible using the current API. Hence, we had to access them using Monkey-Patching *i.e.* we modified the `ExactExplainer` class so that it stores the LSV as one of its attributes. The attribute can then be accessed as seen in Figure 7. The code is provided as a fork the `SHAP` repository. [3]. For the `TreeExplainer`, because its source code is in C++ and wrapped in Python, we found it simpler to simply rewrite our own version of the algorithm in C++ so that it directly returns the LSV, instead of Monkey-Patching the `TreeExplainer`.

```
# Mask features using the whole background distribution
mask = Independent(D_1, max_samples=len(D_1))
explainer = shap.explainers.Exact(model.predict_proba, mask)
# Explain all instances sampled from the foreground
explainer(S_0)
# The LSV are extracted with Monkey-Patching
LSV = explainer.LSV         # LSV.shape = (n_features, |S_0|, |D_1|)
Phi_S_0_zj = LSV.mean(1).T  # Phi_S_0_zj.shape = (|D_1|, n_features)
```

Figure 7: How we extract the LSV from the `ExactExplainer` via Monkey-Patching.

[3] `https://github.com/gablabc/shap/tree/biased_sampling`

C STATISTICAL TESTS

C.1 KS TEST

A first test that can be conducted is a two-samples Kolmogorov-Smirnov (KS) test (Massey Jr, 1951). If we let

$$\widehat{F}_S(x) = \frac{1}{|S|} \sum_{z \in S} \mathbb{1}(z \leqslant x) \tag{33}$$

be the empirical CDF of observations in the set S. Given two sets S and S', the KS statistic is

$$\text{KS}(S, S') = \sup_{x \in \mathbb{R}} |\widehat{F}_S(x) - \widehat{F}_{S'}(x)|. \tag{34}$$

Under the null-hypothesis $H_0 : S \sim \mathcal{D}^{|S|}, S' \sim \mathcal{D}^{|S'|}$ for some univariate distribution $\mathcal{D}$, this statistic is expected to not be too large with high probability. Hence, when the company provides the subsets S'_0, S'_1, the audit can sample their own two subsets $f(S_0), f(S_1)$ uniformly at random from $f(D_0), f(D_1)$ and compute the statistics $\text{KS}(f(S_1), f(S'_1))$ and $\text{KS}(f(S_0), f(S'_0))$ to detect a fraud.

C.2 WALD TEST

An alternative is the Wald test, which is based on the central limit theorem. If $S_1 \sim \mathcal{B}^M$, then the empirical average of the model output over S_1 is asymptotically normally distributed as M increases i.e.

$$\text{Wald}(f(S_1), f(\mathcal{B})) := \frac{\frac{1}{M} \sum_{z \in f(S_1)} z - \mu}{\sigma / \sqrt{M}} \rightsquigarrow \mathcal{N}(0, 1), \tag{35}$$

where $\mu := \mathbb{E}_{z \sim f(\mathcal{B})}[z]$ and $\sigma^2 := \mathbb{V}_{z \sim f(\mathcal{B})}[z]$ are the expected value and variance of the model output across the whole background. The same reasoning holds for S_0 and the foreground $\mathcal{F}$. Applying the Wald test with significance α would detect a fraud when

$$|\,\text{Wald}(f(S'_1), f(\mathcal{B}))\,| > F^{-1}_{\mathcal{N}(0,1)}(1 - \alpha/2), \tag{36}$$

where $F^{-1}_{\mathcal{N}(0,1)}$ is the inverse of the CDF of a standard normal variable.

D METHODOLOGICAL DETAILS

D.1 TOY EXAMPLE

The toy dataset was constructed to closely match the results of the following empirical study comparing skeletal mass distributions between men and women (Janssen et al., 2000). First of, the sex feature was sampled from a Bernoulli

$$S \sim \text{Bernoulli}(0.5). \tag{37}$$

According to the Table 1 of Janssen et al. (2000), the average height of women participants was 163 cm while it was 177cm for men. Both height distributions had the same standard deviation of 7cm. Hence we sampled height via

$$\begin{aligned} H|S = \texttt{man} &\sim \mathcal{N}(177, 49) \\ H|S = \texttt{woman} &\sim \mathcal{N}(163, 49) \end{aligned} \tag{38}$$

It was noted in Janssen et al. (2000) that there was approximately a linear relationship between height and skeletal muscle mass for both sexes. Therefore, we computed the muscle mass M as

$$\begin{aligned} &M|\{H = h, S = \text{man}\} = 0.186h + 5\epsilon \\ &M|\{H = h, S = \text{woman}\} = 0.128h + 4\epsilon \\ &\text{with } \epsilon \sim \mathcal{N}(0, 1) \end{aligned} \tag{39}$$

The values of coefficients 0.186, 0.128 and noise levels 5 and 4 were chosen so the distributions of $M|S$ would approximately match that of Table 1 in Janssen et al. (2000). Finally the target was chosen following

$$\begin{aligned} &Y|\{H = h, M = m\} \sim \text{Bernoulli}(\, P(H, M)\,) \\ &\text{with } P(H, M) = \left[1 + \exp\{100 \times \mathbb{1}(H < 160) - 0.3(M - 28)\}\right]^{-1}. \end{aligned} \tag{40}$$

Simply put, the chances of being hired in the past (Y) were impossible for individuals with a smaller height than 160cm. Moreover, individuals with a higher mass skeletal mass were given more chances to be admitted. Yet, individuals with less muscle mass could still be given the job if they displayed sufficient determination. In the end we generated 6000 samples leading to the following disparity in Y

$$\mathbb{P}(Y = 1|S = \text{man}) = 0.733 \qquad \mathbb{P}(Y = 1|S = \text{woman}) = 0.110. \tag{41}$$

Table 2: Models Test Accuracy % (mean $\pm$ stddev).

	mlp	rf	xgb
COMPAS	68.2 ± 0.9	67.7 ± 0.8	68.6 ± 0.8
Adult	85.6 ± 0.3	86.3 ± 0.2	87.1 ± 0.1
Marketing		91.1 ± 0.1	91.4 ± 0.3
Communities		83 ± 2	82 ± 2

Table 3: Models Demographic Parity (mean $\pm$ stddev).

	mlp	rf	xgb
COMPAS	-0.12 ± 0.01	-0.11 ± 0.01	-0.11 ± 0.02
Adult	-0.20 ± 0.01	-0.19 ± 0.01	-0.192 ± 0.004
Marketing		-0.104 ± 0.005	-0.11 ± 0.01
Communities		-0.50 ± 0.01	-0.54 ± 0.02

D.2 Real Data

The datasets were first divided into train/test subsets with ratio $\frac{4}{5} : \frac{1}{5}$. The models were trained on the training set and evaluated on the test set. All categorical features for COMPAS, Adult, and Marketing were one-hot-encoded which resulted in a total of 11, 40, and 61 columns for each dataset respectively. A simple 50 steps random search was conducted to fine-tune the hyper-parameters with cross-validation on the training set. The resulting test set performance and demographic parities for all models and datasets, aggregated over 5 random data splits, are reported in Tables 2 and 3 respectively.

E ADDITIONAL RESULTS

E.1 MULTIPLE SENSITIVE ATTRIBUTES

We present preliminary results for settings where one wishes to manipulate the Shapley values of multiple sensitive features s each part of a set $s \in \mathcal{S}$. For example, in our experiments we considered `gender` as a sensitive attribute for the Adult-Income dataset and we showed that one can diminish the attribution of this feature. Nonetheless, there are two other features in Adult-Income that share information with this `gender`: `relationship` and `marital-status`. Indeed, `relationship` can take the value `widowed` and `marital-status` can take the value `wife`, which are both proxies of `gender=female`. For this reason, these two other features may be considered sensitive and decision-making that relies strongly on them may not be acceptable. Henceforth, we must derive a method that reduces the total attributions of the features in $\mathcal{S} = \{\texttt{gender}, \texttt{relationship}, \texttt{marital-status}\}$.

We first let $\beta_s := \text{sign}[\,\widehat{\Phi}_s(f, S'_0, D_1)\,]$ for any $s \in \mathcal{S}$. In our experiments, all these signs will typically be negative. The proposed approach is to minimize the ℓ_1 norm

$$\|(\widehat{\Phi}_s(f, S'_0, S'_1))_{s\in\mathcal{S}}\|_1 := \sum_{s\in\mathcal{S}} |\,\widehat{\Phi}_s(f, S'_0, S'_1)\,|, \tag{42}$$

which we interpret as the total amount of disparity we can attribute to the sensitive attributes. Remember that $\widehat{\Phi}_s(f, S'_0, S'_1)$ converges in probability to $\sum_{\boldsymbol{z}^{(j)}\in D_1} \omega_j\, \widehat{\Phi}_s(f, S'_0, \boldsymbol{z}^{(j)})$ (cf. Proposition 4.1). Therefore minimizing the ℓ_1 norm will require minimizing

$$\sum_{s\in\mathcal{S}} \beta_s \sum_{\boldsymbol{z}^{(j)}\in D_1} \omega_j\, \widehat{\Phi}_s(f, S'_0, \boldsymbol{z}^{(j)}) = \sum_{\boldsymbol{z}^{(j)}\in D_1} \omega_j \sum_{s\in\mathcal{S}} \beta_s\, \widehat{\Phi}_s(f, S'_0, \boldsymbol{z}^{(j)}), \tag{43}$$

which is again a linear function of the weights. We present Algorithm 4 as an overload of Algorithm 1 that now supports taking multiple sensitive attributes as inputs.

Algorithm 4 Compute non-uniform weights for multiple sensitive attributes $s \in \mathcal{S}$

1: **procedure** COMPUTE_WEIGHTS($D_1, \{\widehat{\Phi}_s(f, S'_0, \boldsymbol{z}^{(j)})\}_{s,j}, \lambda$)
2: $\quad\beta_s := \text{sign}[\sum_{\boldsymbol{z}^{(j)}\in D_1} \widehat{\Phi}_s(f, S'_0, \boldsymbol{z}^{(j)})\,]\ \ \forall s \in \mathcal{S}$;
3: $\quad\mathcal{B} := \mathcal{C}(D_1, \mathbf{1}/N_1)$ ▷ Unmanipulated background
4: $\quad\mathcal{B}'_{\boldsymbol{\omega}} := \mathcal{C}(D_1, \boldsymbol{\omega})$ ▷ Manipulated background as a function of $\boldsymbol{\omega}$
5: $\quad\boldsymbol{\omega} = \arg\min_{\boldsymbol{\omega}}\ \sum_{\boldsymbol{z}^{(j)}\in D_1} \omega_j \sum_{s\in\mathcal{S}} \beta_s\, \widehat{\Phi}_s(f, S'_0, \boldsymbol{z}^{(j)}) + \lambda\mathcal{W}(\mathcal{B}, \mathcal{B}'_{\boldsymbol{\omega}})$
6: $\quad$**return** $\boldsymbol{\omega}$;

The only difference in the resulting MCF is that we must use the cost $a(e) = \sum_{s\in\mathcal{S}} \beta_s\, \widehat{\Phi}_s(f, S'_0, \boldsymbol{z}^{(j)})$ for edges (s, ℓ_j) in the graph $\mathbb{G}$ of Figure 6. This new algorithm is guaranteed to diminish the ℓ_1 norm of the attributions of all sensitive features. However, that this does not imply that all sensitive attributes will diminish in amplitude. Indeed, minimizing the sum of multiple quantities does not guarantee that each quantity will diminish. For example, $4 + 7$ is smaller than $6 + 6$ although 4 is smaller than 6 and 7 is higher than 6. Still, we see reducing the ℓ_1 norm as a natural way to hide the total amount of disparity that is attributable to the sensitive features. Another important methodological change is the way we select the optimal hyper-parameter λ in Algorithm 3. Now at line 13, we use the ℓ_1 norm $\sum_{s\in\mathcal{S}} |\sum_{\boldsymbol{z}^{(j)}\in D_1} \omega_j\, \widehat{\Phi}_s(f, S'_0, \boldsymbol{z}^{(j)})|$ as a selection criterion.

Figures 8 and 9 present preliminary results of attacks on three RFs/XGBs fitted on Adults with different train/test splits. We note that in all cases, before the attack, the three sensitive features had large negative attributions. By applying our method, we can considerably reduce the amplitude of the two sensitive attributes. The attribution of the remaining sensitive feature remains approximately constant or slightly becomes more negative. We leave it as future work to run large scale experiments with multiple sensitive features for various datasets.

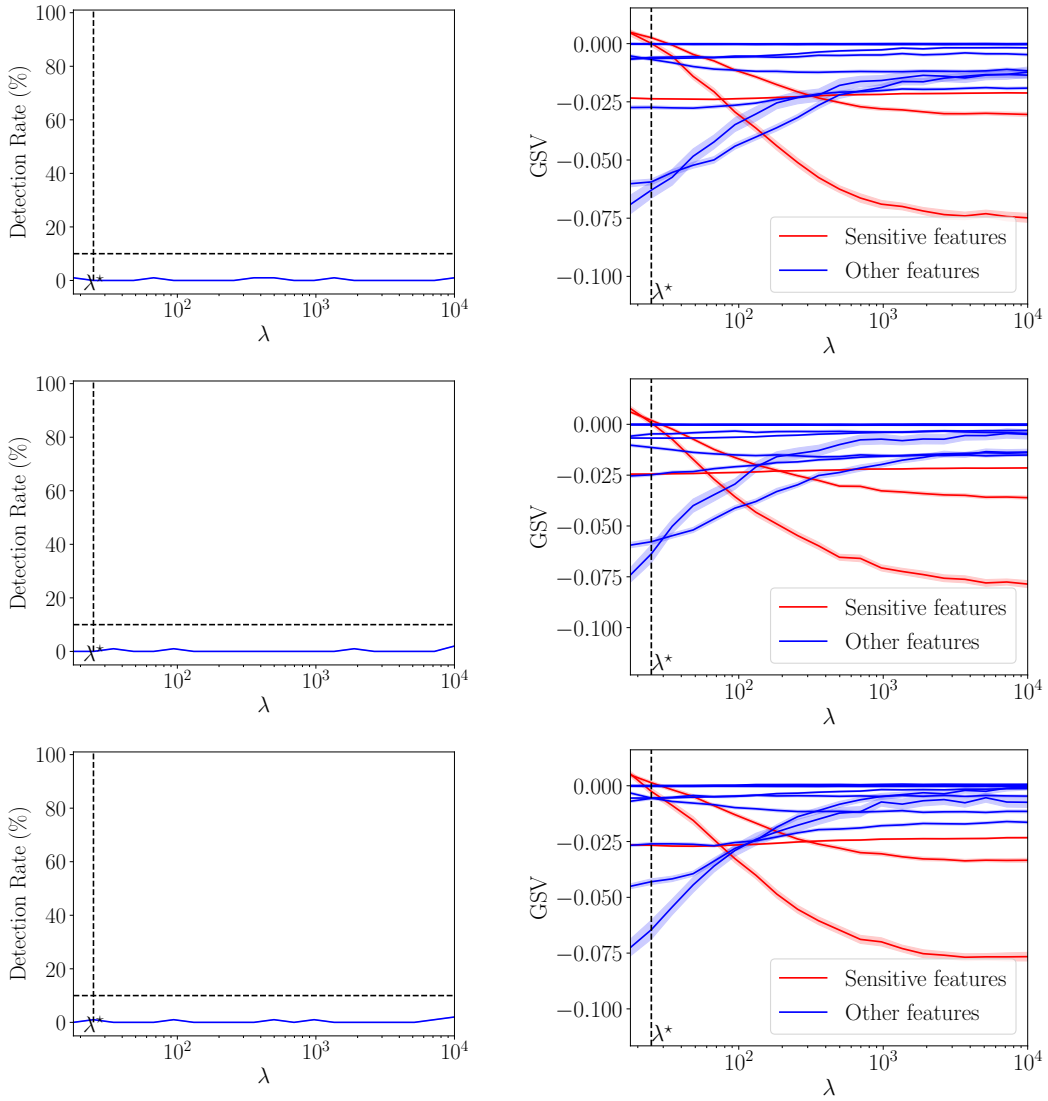

Figure 8: Example of log-space search over values of λ using RFs classifier fitted on Adults and three sensitive attributes. Each row is a different train/test split seed. (Left) The detection rate as a function of the parameter λ of the attack. (Right) For each value of λ, the vertical slice of the 11 curves is the GSV obtained with the resulting $\mathcal{B}'_\omega$. The goal here is to reduce the amplitude all sensitive features (red curves) in order to hide their contribution to the disparity in model outcomes.

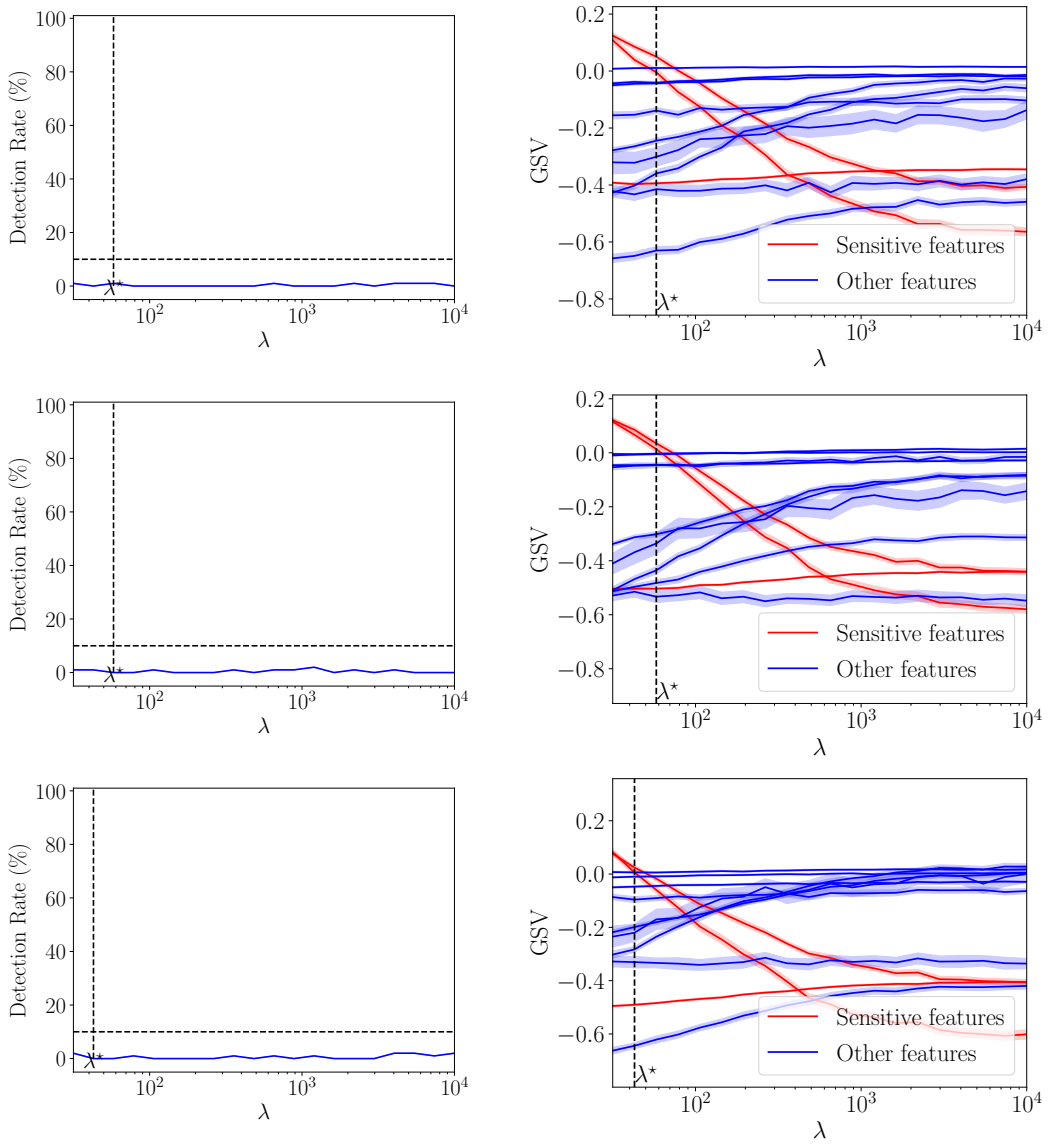

Figure 9: Example of log-space search over values of λ using XGBs classifier fitted on Adults and three sensitive attributes. Each row is a different train/test split seed. (Left) The detection rate as a function of the parameter λ of the attack. (Right) For each value of λ, the vertical slice of the 11 curves is the GSV obtained with the resulting $\mathcal{B}'_\omega$. The goal here is to reduce the amplitude all sensitive features (red curves) in order to hide their contribution to the disparity in model outcomes.

E.2 Examples of Attacks

In this section, we present 8 specific examples of the attacks that were conducted on COMPAS, Adult, Marketing, and Communities.

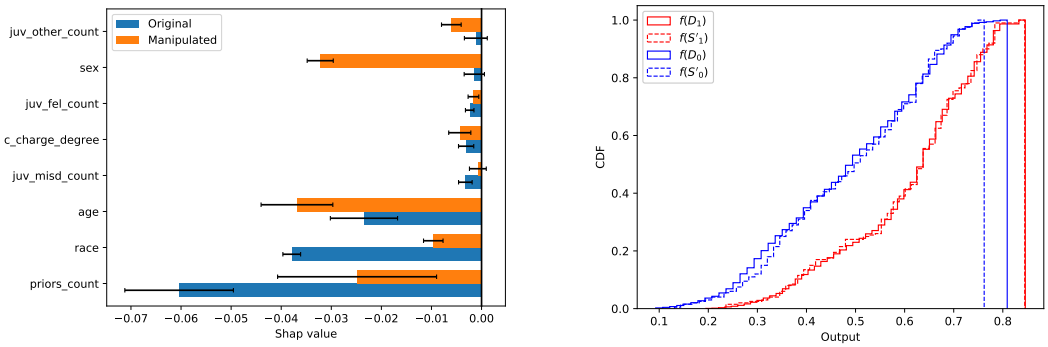

Figure 10: Attack of RF fitted on COMPAS. Left: GSV before and after the attack with $M = 200$. As a reminder, the sensitive attribute is `race`. Right: Comparison of the CDF of the misleading subsets $f(S'_0), f(S'_1)$ and the CDF over the whole data. $f(D_0), f(D_1)$.

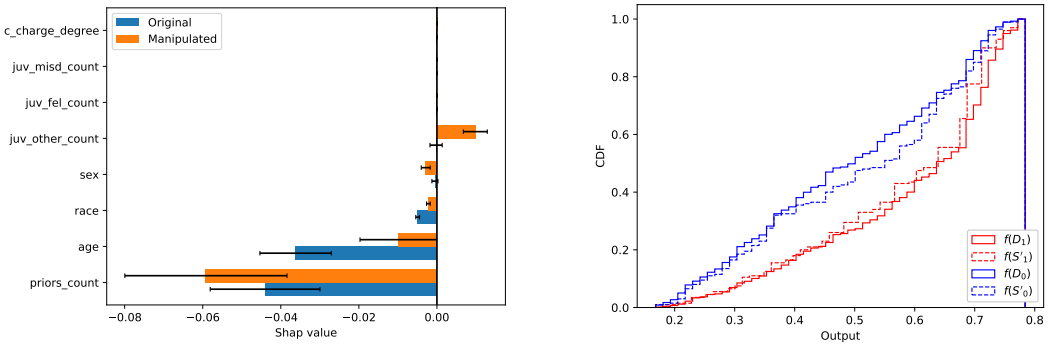

Figure 11: Attack of XGB fitted on COMPAS. Left: GSV before and after the attack with $M = 200$. As a reminder, the sensitive attribute is `race`. Right: Comparison of the CDF of the misleading subsets $f(S'_0), f(S'_1)$ and the CDF over the whole data. $f(D_0), f(D_1)$.

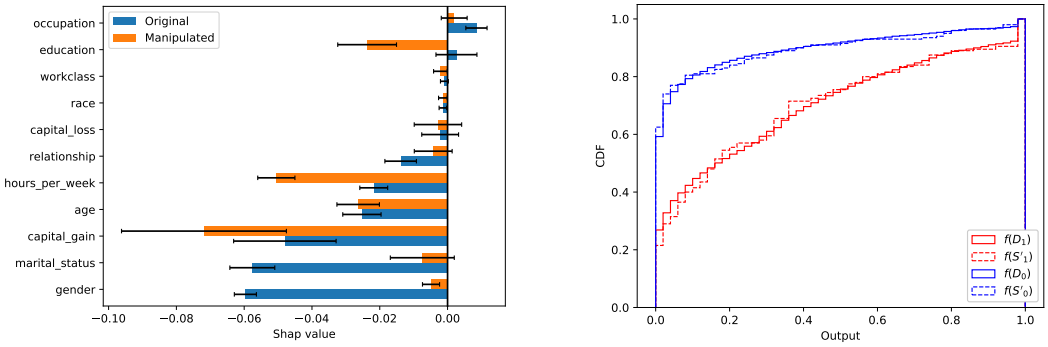

Figure 12: Attack of XGB fitted on Adults. Left: GSV before and after the attack with $M = 200$. As a reminder, the sensitive attribute is `gender`. Right: Comparison of the CDF of the misleading subsets $f(S'_0), f(S'_1)$ and the CDF over the whole data. $f(D_0), f(D_1)$.

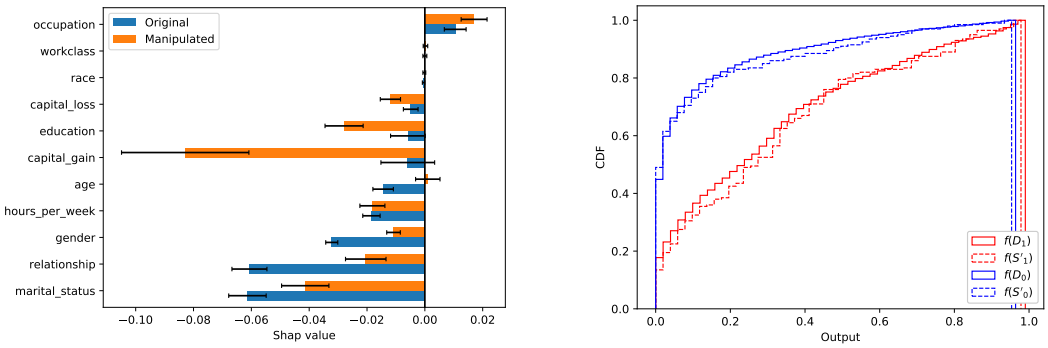

Figure 13: Attack of RF fitted on Adults. Left: GSV before and after the attack with $M = 200$. As a reminder, the sensitive attribute is `gender`. Right: Comparison of the CDF of the misleading subsets $f(S'_0), f(S'_1)$ and the CDF over the whole data. $f(D_0), f(D_1)$.

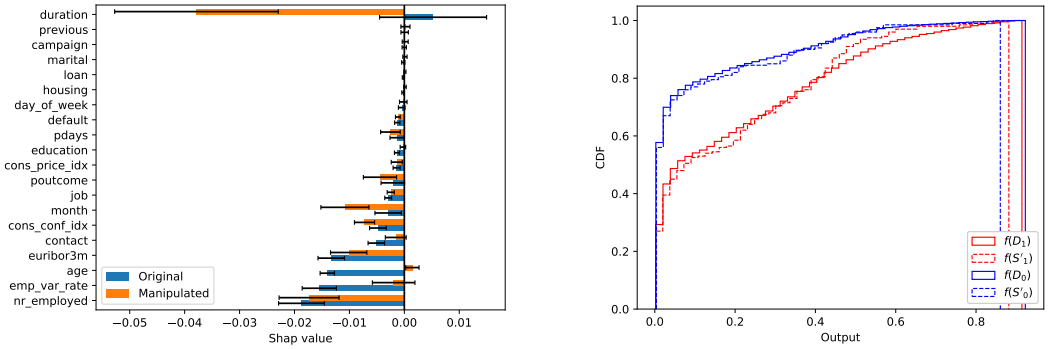

Figure 14: Attack of RF fitted on Marketing. Left: GSV before and after the attack with $M = 200$. As a reminder, the sensitive attribute is `age`. Right: Comparison of the CDF of the misleading subsets $f(S'_0), f(S'_1)$ and the CDF over the whole data. $f(D_0), f(D_1)$.

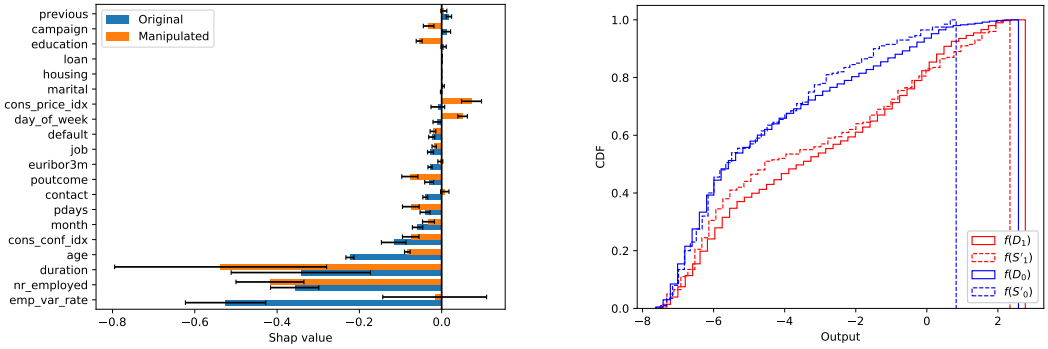

Figure 15: Attack of XGB fitted on Marketing. Left: GSV before and after the attack with $M = 200$. As a reminder, the sensitive attribute is `age`. Right: Comparison of the CDF of the misleading subsets $f(S'_0), f(S'_1)$ and the CDF over the whole data. $f(D_0), f(D_1)$. Since we used the `TreeExplainer` for this model, we had to explain its raw output which is a logit and not a probability. Hence the output is not constrained to the interval $[0, 1]$.

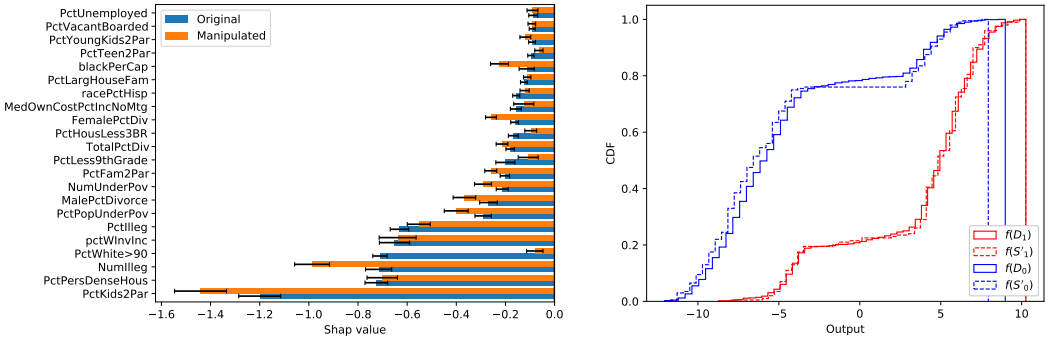

Figure 16: Attack of XGB fitted on Communities. Left: GSV before and after the attack with $M = 200$. As a reminder, the sensitive attribute is `PctWhite>90`. Right: Comparison of the CDF of the misleading subsets $f(S'_0), f(S'_1)$ and the CDF over the whole data. $f(D_0), f(D_1)$. Since we used the `TreeExplainer` for this model, we had to explain its raw output which is a logit and not a probability. Hence the output is not constrained to the interval $[0, 1]$.

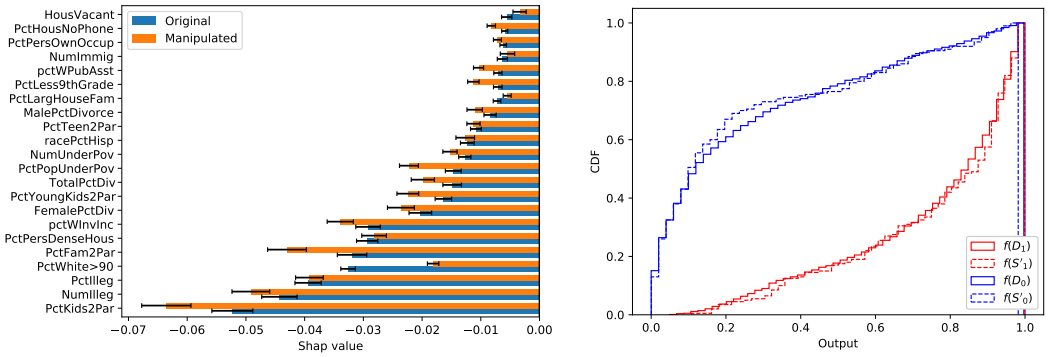

Figure 17: Attack of RF fitted on Communities. Left: GSV before and after the attack with $M = 200$. As a reminder, the sensitive attribute is `PctWhite>90`. Right: Comparison of the CDF of the misleading subsets $f(S'_0), f(S'_1)$ and the CDF over the whole data. $f(D_0), f(D_1)$.